



Contents lists available at ScienceDirect

# Physics of the Earth and Planetary Interiors

journal homepage: [www.elsevier.com/locate/pepi](http://www.elsevier.com/locate/pepi)

## 3-D crustal velocity structure of western Turkey: Constraints from full-waveform tomography

Yeşim Çubuk-Sabuncu<sup>a,\*</sup>, Tuncay Taymaz<sup>a</sup>, Andreas Fichtner<sup>b</sup><sup>a</sup> Istanbul Technical University, Department of Geophysical Engineering, The Faculty of Mines, Maslak 34469, Istanbul, Turkey<sup>b</sup> ETH Zurich, Institute of Geophysics, Sonneggstrasse 5, CH-8092 Zurich, Switzerland

### ARTICLE INFO

#### Article history:

Received 24 March 2017

Received in revised form 30 June 2017

Accepted 30 June 2017

Available online 3 July 2017

#### Keywords:

Computational seismology

Seismic anisotropy

Full-waveform tomography

Turkey

### ABSTRACT

The Sea of Marmara and western Turkey are characterized by intense seismicity and crustal deformation due to transition tectonics between the North Anatolian Fault Zone (NAFZ) and the extensional Aegean. Seismic imaging of the crust and uppermost mantle in W-NW Turkey is crucial to obtain a better understanding of its seismotectonics and geodynamics. So far, the Sea of Marmara and surroundings were considered in various active and passive seismic experiments providing significant information on crustal properties. Here, we further investigate the 3-D seismic velocity structure in this rapidly deforming region using non-linear full-waveform tomography based on the adjoint method. Our model is constrained by complete waveforms of 62 regional earthquakes (epicentral distance  $< 10^\circ$ ) with magnitudes  $M_w \geq 3.7$ , which occurred between 2007 and 2015. Validation tests show that our final 3-D Earth model is able to explain seismic waveforms from earthquakes not used in the inversion at periods from 8–100 s to within the data uncertainties. Furthermore, quantitative resolution analyses yield 15 to 35 km horizontal resolution lengths in the shallow and deep crust beneath well-covered areas of W-NW Turkey. Our full-waveform tomography results indicate the presence of strong lateral and vertical velocity variations ( $2.55 \leq V_s \leq 4.0$  km/s) down to depths of  $\sim 35$  km. The seismic velocity distribution is characteristic of highly deformed and distributed crustal features along major fault zones (e.g. NAFZ and its branches), historic and recent regional volcanism (e.g. Kula volcanic province), and metamorphic core complex developments (e.g. Menderes and Kazdağ massifs). Radial anisotropy is very strong (around 20%) throughout the crust, further attesting to strong deformation and heterogeneity. Generally, our 3-D model is overall consistent with the active tectonics of western Turkey.

© 2017 Elsevier B.V. All rights reserved.

## 1. Introduction

### 1.1. The Aegean extensional domain – western Turkey

The active tectonics of Turkey are the result of interactions between continental collision of the Arabian plate with the Eurasian plate in the east, and subduction of the African plate beneath the Aegean (McKenzie, 1972; Dewey et al., 1986; Meulenkamp et al., 1988; Taymaz et al., 1991, 2007; Endrun et al., 2011; Fielding et al., 2013; Yolsal-Çevikbilen et al., 2014). These tectonic motions have an important role in the development of the westward extrusion of Turkey, which is accommodated by the North Anatolian Fault Zone (NAFZ), and ongoing lithospheric-scale extension due to trench roll-back in the Hellenic subduction zone

(Taymaz et al., 1990; Confal et al., 2016). As a consequence, the extensional deformation in the North Aegean and the Sea of Marmara is combined with strike-slip tectonics. This leads to an unusually complex tectonic framework, summarized in Fig. 1. Expressions of this complexity include intense seismicity along the right-lateral strike-slip NAFZ, and volcanism in the Aegean extensional domain.

Structural complexities with different rock and basement types in western Turkey evolved due to continental collision, ophiolite formation, subduction dynamics, continental extension, magmatism, and core complex developments. In this framework, major tectonic structures in W-NW Turkey include the following: [1] The right-lateral strike slip North Anatolian Fault Zone (NAFZ), and its three branches towards to west around  $31^\circ\text{E}$ , which result from the interaction with the extensional Aegean (McKenzie, 1972; Şengör, 1979; Şengör et al., 1985; Taymaz, 1996; Taymaz et al., 2004; Taymaz et al., 2007). [2] The Intra-Pontide Suture Zone (IPSZ), which represents the boundary between the Strandja Massif

\* Corresponding author.

E-mail addresses: [cubuky@itu.edu.tr](mailto:cubuky@itu.edu.tr) (Y. Çubuk-Sabuncu), [taymaz@itu.edu.tr](mailto:taymaz@itu.edu.tr) (T. Taymaz), [andreas.fichtner@erdw.ethz.ch](mailto:andreas.fichtner@erdw.ethz.ch) (A. Fichtner).

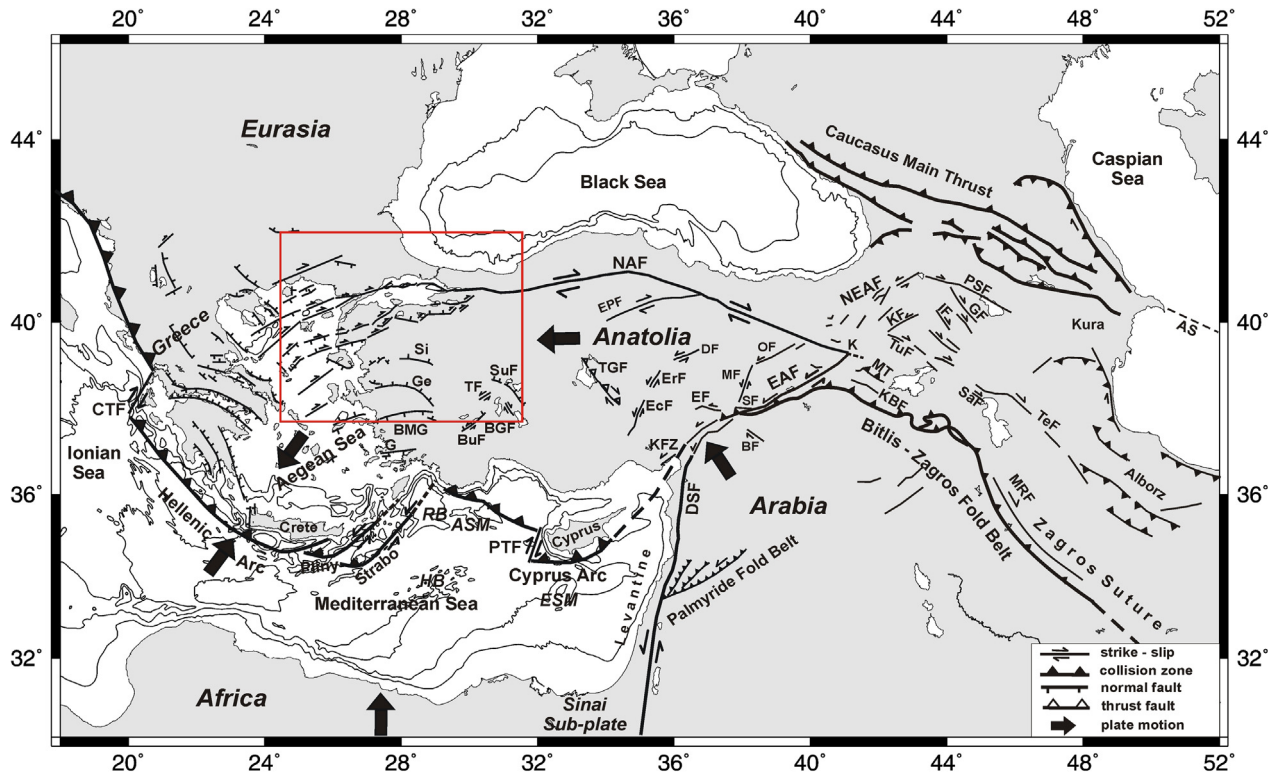


**Fig. 1.** Active tectonic boundaries in the study area and surroundings, compiled from Mascle and Martin (1990), Taymaz et al. (1990, 1991, 2004, 2007), Şaroğlu et al. (1992), Taymaz and Price (1992), Taymaz (1996), Aksu et al. (2008), Hall et al. (2008), Yolsal (2008), Yolsal-Çevikbilen and Taymaz (2012), Yolsal-Çevikbilen et al. (2012, 2014), Yolsal-Çevikbilen (2014) and Çubuk et al. (2014). Abbreviations: AS: Apşeron Sili, ASM: Anaximander Sea Mountains, BF: Bozova Fault, BGF: Beyşehir Gölü Fault, BMG: Büyük Menderes Graben, BuF: Burdur Fault, CTF: Cephalonia Transform Fault, DSF: Dead Sea Transform Fault, DF: Deliler Fault, EAF: East Anatolian Fault, EcF: Eciş Fault, EF: Elbistan Fault, EPF: Ezine Pazarı Fault, ErF: Erciyes Fault, ESM: Eratosthenes Sea Mountains, G: Gökova, Ge: Gediz Graben, GF: Garni Fault, HB: Herodotus Basin, IF: Iğdır Fault, KBF: Kavakbaşı Fault, KF: Kağızman Fault, KFZ: Karataş-Osmaniye Fault Zone, MF: Malatya Fault, MRF: Main Recent Fault, MT: Muş Thrust, NAF: North Anatolian Fault, NEAF: North East Anatolian Fault, OF: Ovacık Fault, PSF: Pampak-Savan Fault, PTF: Paphos Transform Fault, RB: Rhodes Basin, SaF: Salmas Basin, Si: Simav Graben, SuF: Sultandağ Fault, TeF: Tebriz Fault, TF: Tatarlı Fault, TGF: Tuz Gölü Fault. Black arrows exhibit relative plate motions with respect to Eurasia (McClusky et al., 2003; Reilinger et al., 2006). Bathymetric contours are shown at 1000 m, 1500 m and 2000 m, and are obtained from GEBCO-BODC (1997). The red box outlines the study area.

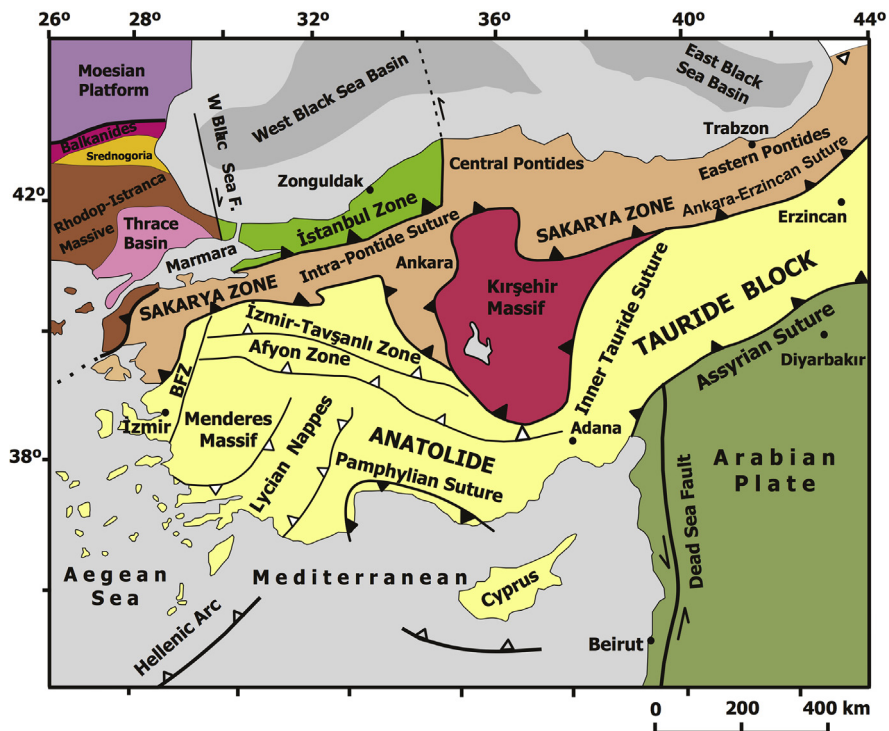


**Fig. 2.** Tectonic sketch map of Turkey (replotted from Okay and Tüysüz, 1999; Okay, 2008). Main suture zones are displayed with thick black lines. Former and current subduction zones are marked with filled and open black triangles, respectively.

(SM), the İstanbul (İZ) and Sakarya zones (SZ) (Okay and Tüysüz, 1999; Okay and Satır, 2006). The İZ has a Precambrian crystalline basement, while metamorphic basement units, the Karakaya Complex, and Oligo-Miocene granitoids mainly characterize the SZ (e.g. Kazdağ and Uludağ massifs, Çataldağ granitoid). [3] The İzmir-Ankara-Erzincan suture zone (IAESZ) defines a collision and magmatic boundary between the SZ and the Anatolide–Tauride Platform (ATP) (Şengör and Yılmaz, 1981; Okay and Tüysüz, 1999). [4] In the south, the Anatolide-Tauride block consists of metamorphic (e.g. Menderes Massif) and volcano-sedimentary units (van Hinsbergen et al., 2010; Altunkaynak et al., 2012). Numerous E-W oriented horst-graben systems developed in this region as a result of the extensional tectonics (e.g. Gediz, Büyük Menderes, Küçük Menderes, Simav). These abovementioned tectonic structures are presented in a simplified tectonic sketch (Fig. 2). The distribution of the regional geologic features is subsequently presented in Fig. 3.

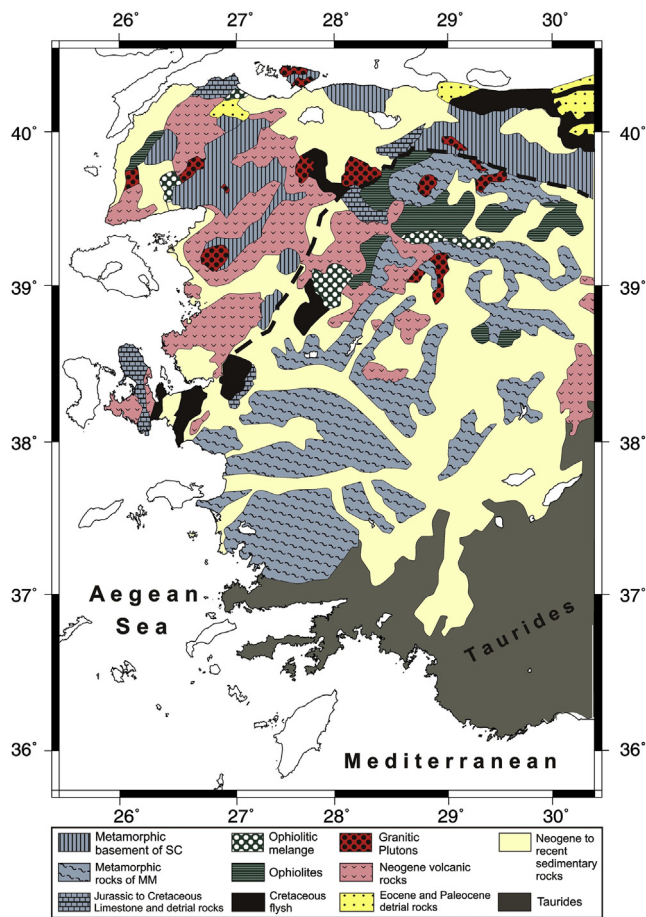


Fig. 3. Regional geological units of western Turkey (replotted from Yılmaz et al. (2000)). Abbreviations: SC: Sakarya Continent, MM: Menderes Massif.

While the subsurface structure in relation to active tectonics has long been studied, recent advances in computational seismology now allow us to obtain a yet more detailed image of the complex crust beneath W-NW Turkey. In this paper, we describe a new 3-D radially anisotropic shear wave velocity model of western Turkey built with full-waveform tomography, which allows us to optimally exploit the available regional seismic data. Our model provides new insight into the seismic velocity and anisotropy characteristics of the crust and uppermost mantle beneath the Sea of Marmara and western Turkey.

## 1.2. Outline

With the objective to present a new 3-D radially anisotropic shear wave velocity model of the crust and uppermost mantle of W-NW Turkey, this paper is organized as follows: First, we describe the characteristics and the selection of seismic data. Subsequently, we briefly review the full-waveform tomography method to construct 3-D Earth models. We then present waveform fitting and quantitative resolution tests in the model analysis section. We describe the main features of the 3-D Earth model separately for the isotropic S velocities, SH and SV velocities, and radial anisotropy. This is followed by a detailed discussion on the likely causes of the observed seismic velocity anomalies and radial anisotropy patterns. Additional waveform fits, final 3-D crustal velocity model parameters and movies showing the model variations with depth are presented as online [Supplementary Material](#).

## 2. Data

We used three-component complete waveforms from earthquakes that occurred during 2007–2015 in order to constrain the 3-D crustal structure of W-NW Turkey. The data primarily originated from the broadband stations of the Boğaziçi University-Kandilli Observatory and Earthquake Research Institute (BU-KOERI, Turkey, 50 stations). We also used 4 broadband stations of the Disaster and Emergency Management Presidency, Earthquake Department (AFAD-ERD, Turkey). Additional broadband stations that are located within the study region and operated by the Hellenic Unified Seismic Network (HUSN, Greece, 4 stations) and the GEOFON Program (Germany) also provided regional earthquake data (epicentral distance  $\Delta < 10^\circ$ ). The distribution of the seismic broadband stations is shown in Fig. 4. Based on a visual quality assessment, we selected and simulated velocity recordings with significant signal amplitudes above the background noise. To maximize tomographic resolution, we exploited all seismic phases, including body waves, surface waves and interfering phases on all three components. We filtered observed and synthetic data in a frequency band of 0.01–0.125 Hz (8–100 s), which allows us to jointly resolve crustal and uppermost mantle structure. Our dataset consists of moderate-size earthquakes ( $3.7 \leq M_w \leq 5.9$ ), allowing us to neglect finite-source effects. We principally obtained earthquake locations from the International Seismological Centre (ISC) database. Earthquake source mechanisms and corresponding moment magnitudes originate from the Institute of Geodynamics of the National Observatory of Athens (NOA-IG), the Global Centroid Moment Tensor Catalog (GCMT), the Disaster and Emergency Management Presidency, Earthquake Department (AFAD-ERC) and the Kandilli Observatory and Earthquake Research Institute (BU-KOERI) databases. To exclude potentially unreliable source mechanism solutions, we selected moment tensor inversion results with a variance reduction of  $>50\%$ , a double couple value of  $>50\%$ , and a compensated linear vector dipole of  $<20\%$ . To ensure the efficiency of the adjoint method (Tarantola, 1984; Fichtner et al., 2009a), we restricted ourselves to earthquakes recorded by at least 10 different stations.

The revised dataset contains 2/985 recordings from 62 earthquakes, distributed throughout the region. The ray coverage is shown in Fig. 5.

## 3. Full-waveform tomography

### 3.1. Technical details

Full-waveform tomography – also referred to as full-waveform inversion or adjoint tomography – is a recently developed class of

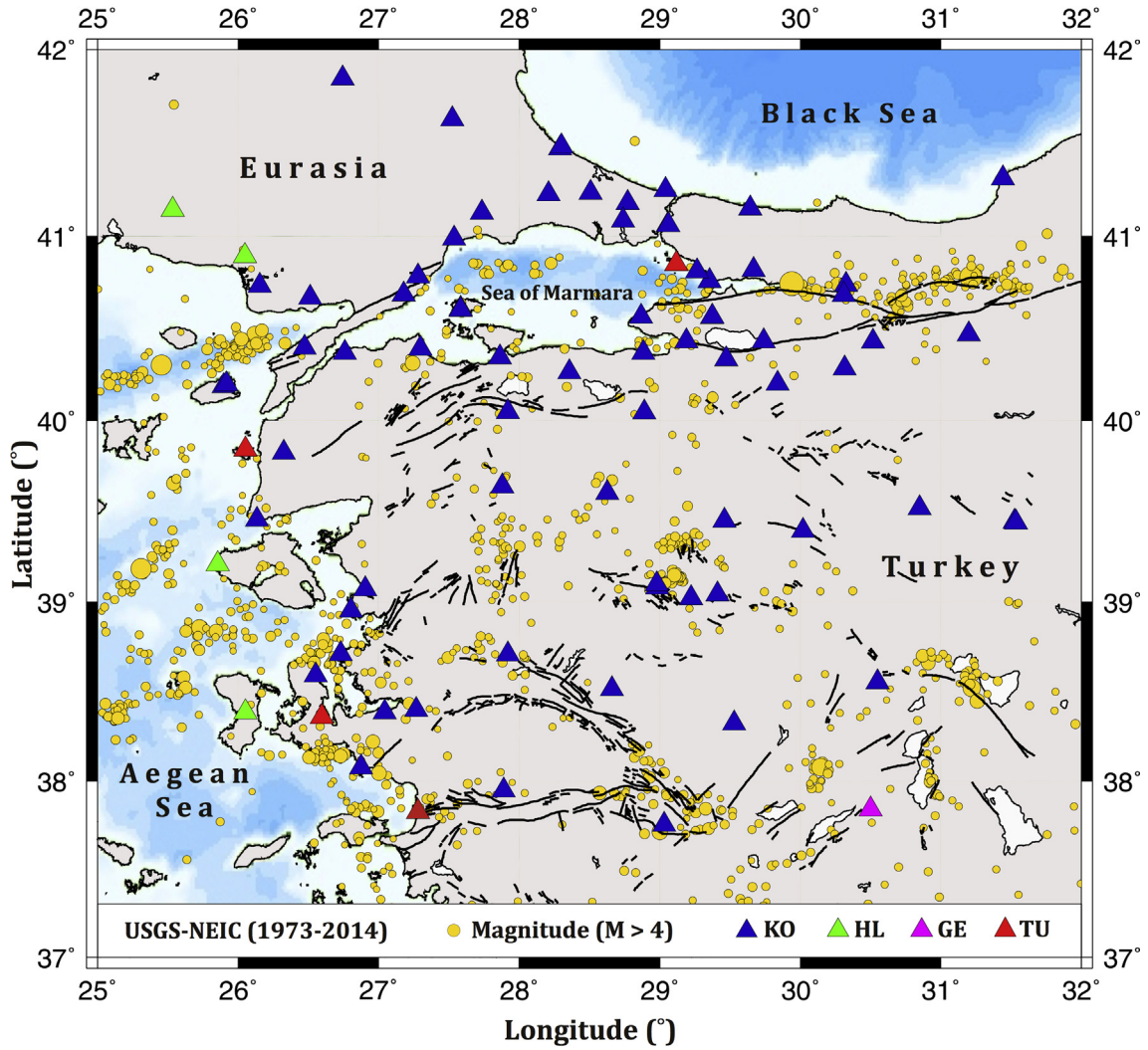


**Fig. 4.** Distribution of seismic broadband stations in the study area. Background seismicity is also shown with yellow circles ( $M \geq 4$ ). Earthquake and bathymetry data are obtained from the USGS-NEIC (1973–2014) and ETOPO1 relief model. Blue and green triangles mark seismic stations of the BU-KOERI and HUSN, while purple and red triangles mark locations of stations within the GEOFON and AFAD-ERC networks, respectively. (For interpretation of the references to colour in this figure legend, the reader is referred to the web version of this article.)

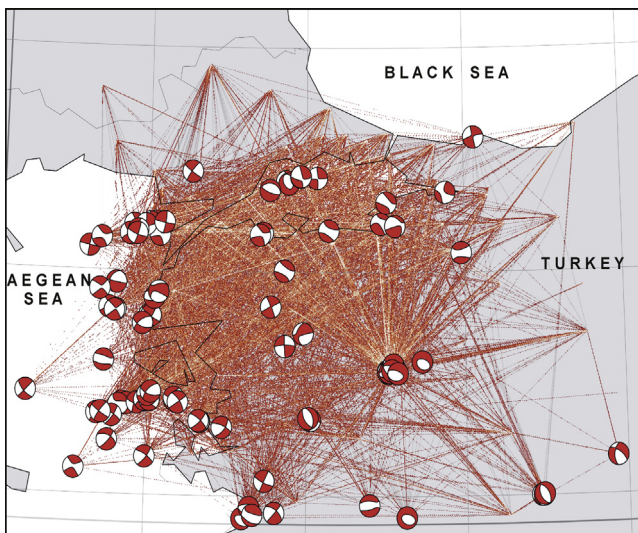


**Fig. 5.** Ray coverage for earthquakes used in this study (2007–2015). Red lines indicate the source-receiver paths. Source mechanisms are located at earthquake epicenters. (For interpretation of the references to colour in this figure legend, the reader is referred to the web version of this article.)

tomographic techniques that allow us to exploit complete seismograms for the benefit of improved resolution (e.g. [Chen et al., 2007](#); [Fichtner et al., 2009a](#); [Tape et al., 2010](#); [Colli et al., 2013](#); [Rickers et al., 2013](#); [Zhu et al., 2015](#)). Numerical solutions of the wave equation ensure that forward modelling errors for complex 3-D Earth models can practically be neglected, and the use of adjoint techniques ([Fichtner et al., 2006a,b](#); [Fichtner et al., 2010](#)) provides the correct finite-frequency sensitivity kernels for any type of measurement that is found to be suitable for a specific dataset.

For this study, we employed the spectral-element solver SES3D to simulate seismic wave propagation through 3-D heterogeneous, anisotropic, visco-elastic Earth models in spherical coordinates ([Fichtner et al., 2009b](#); [Gokhberg and Fichtner, 2016](#)). To prevent unphysical reflections at model boundaries, we implemented anisotropic perfectly matched layers (APMLs; [Teixeira and Chew, 1997](#); [Zheng and Huang, 1997](#)).

To organize both the data and the inversion workflow, we employed the LARge-Scale Seismic Inversion Framework (LASIF; [Krischer et al., 2015](#)). To quantify the discrepancies between observed and synthetic waveforms, we measured time- and frequency-dependent phase misfits ([Fichtner et al., 2008](#)) for any part of the recordings that are clearly above the noise level and

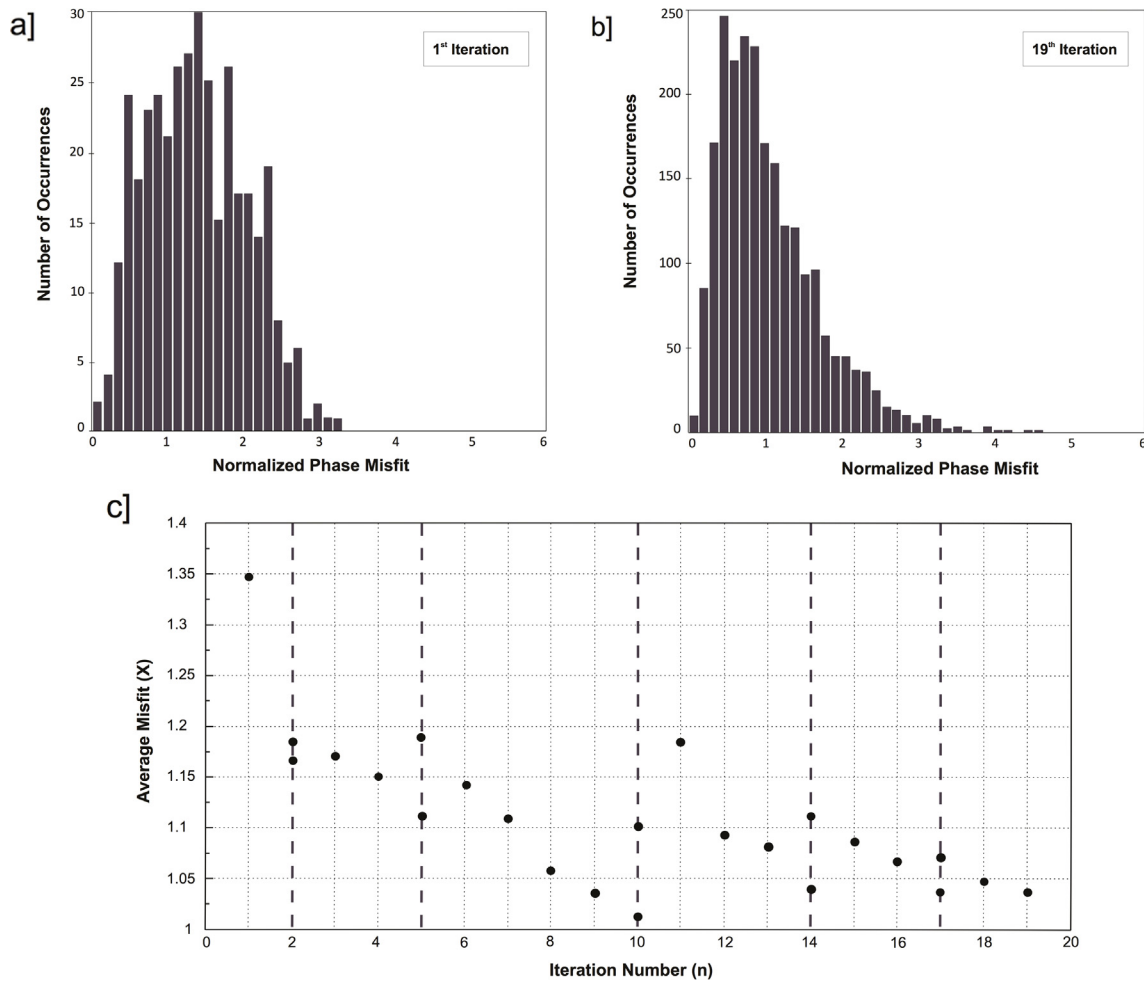


**Fig. 6.** Histograms showing the distribution of phase misfits for the initial and final Earth models. Misfits are normalized with respect to the number of events. a) Relative misfits for the initial model, b) Relative misfits for the final model, c) Evolution of overall relative misfits. We expanded the data set at stages represented with purple dashed lines.

not suffering from obvious cycle skips. We minimized this misfit by updating P velocity, SH velocity, SV velocity, and density, using a non-linear conjugate-gradient algorithm (Hestenes and Stiefel, 1952; Fletcher and Reeves, 1964). The sensitivity kernels needed in the conjugate-gradient iteration were computed with the help of adjoint techniques (Tarantola, 1984; Liu and Tromp, 2006; Fichtner et al., 2006a,b).

### 3.2. Application to western Turkey

Reliable a priori information is crucial to ensure convergence of the iterative inversion towards the global optimum (Kissling et al., 1994; Gao, 2004). We implemented the initial 3-D Earth model from the multi-scale inversion of Fichtner et al. (2013a,b) for Europe and western Asia. Their radially anisotropic model already covers europe western Turkey, though with much less data than our more targeted study. The attenuation model, already included in the initial model, is QL6 by Durek and Ekström (1996).

Our modelling domain ranges from 24 to 33°E longitude, from 37.5 to 43°N latitude, and from the surface to 471 km depth. It is discretized by 69'888 finite elements within which the seismic wavefield is approximated by tensorized polynomials of degree 4. This translates to a total of around 9 million grid points. This setup allows us to model waves with a minimum period of around 8 s with sufficient accuracy, i.e., with modelling errors much smaller than the data uncertainties.

During the inversion, we iteratively updated SH and SV velocity ( $V_{SH}$ ,  $V_{SV}$ ), P velocity ( $V_P$ ), and density ( $\rho$ ). However, since  $V_P$  and  $\rho$  are less resolved by our surface wave-dominated data, they will not be interpreted in this paper.

Since the differences between observed and synthetic waveforms on the 500-km scale are by far dominated by crustal heterogeneities on the order of 10%, we did not perform a joint inversion for earthquake source parameters. However, as explained in the Conclusions, a source inversion will be performed in a future study in order to further improve results.

We stopped the inversion after 19 iterations, because the misfit reduction per iteration became negligibly small, less than 1% of the initial misfit of 1.35. The final misfit was 1.04. Misfit statistics are summarized in Fig. 6. During the inversion, the total number of usable measurement time windows – intervals where observed and synthetic seismograms are sufficiently similar to allow for a meaningful comparison – increased from 368 in the first iteration to 2302 in the final iteration. This increase reflects the successively better match between observations and synthetics that cause a decrease of cycle skips with each iteration.

## 4. Model analysis

Prior to the detailed description and interpretation of our final model, we present an analysis of tomographic resolution, and of

the model's ability to explain seismic waveforms used and not used in the inversion.

#### 4.1. Resolution analysis

We performed a resolution analysis for our 3-D radially anisotropic Earth model following the random probing method developed by Fichtner and van Leeuwen (2015). Resolution analysis by random probing yields position- and direction-dependent resolution lengths, thus being less subjective and more quantitative than synthetic recovery tests.

Resolution lengths in E-W and N-S directions for W-NW Turkey are displayed in Fig. 7. Generally, resolution length varies strongly due to the heterogeneous data coverage. Beneath the most densely covered regions – including the Biga Peninsula, the Menderes Massif, Lesvos Island, the Gulf of Saros, the Sea of Marmara and the Kula Volcanic Province – horizontal resolution reaches around 20 km. This is close to the minimum wavelength, and thus close to the theoretically expected resolution optimum. With increasing depth, the resolved volume decreases because the short epicentral distances used in this study provide little illumination below 30 km depth. Due to the small depth extent of our model,

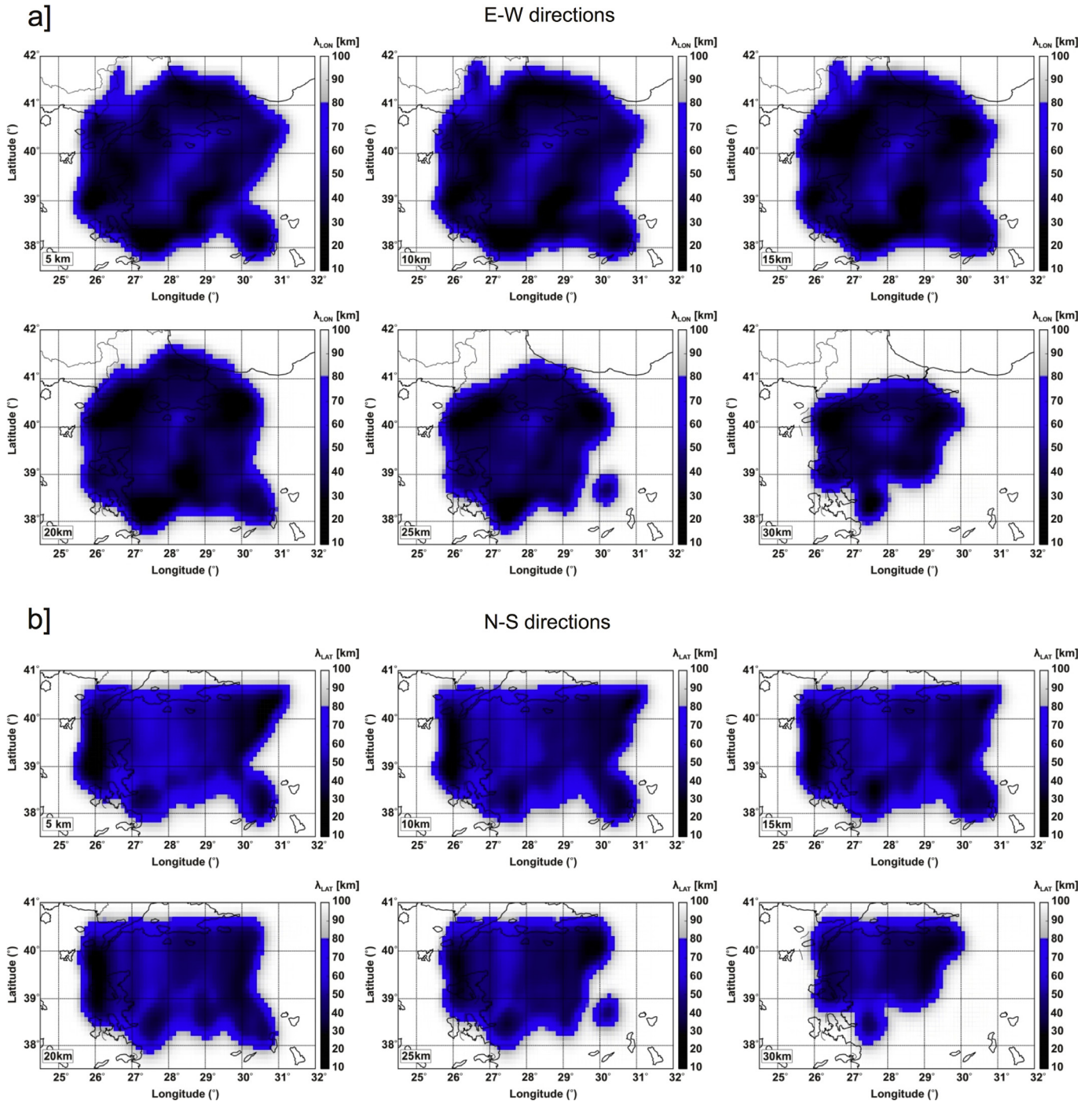


**Fig. 7.** Horizontal depth sections showing position and direction dependent resolution lengths in longitude (E-W) and latitude (N-S) directions for depths of 5 km to 30 km. In each horizontal section, depth information is given in the lower left corner.

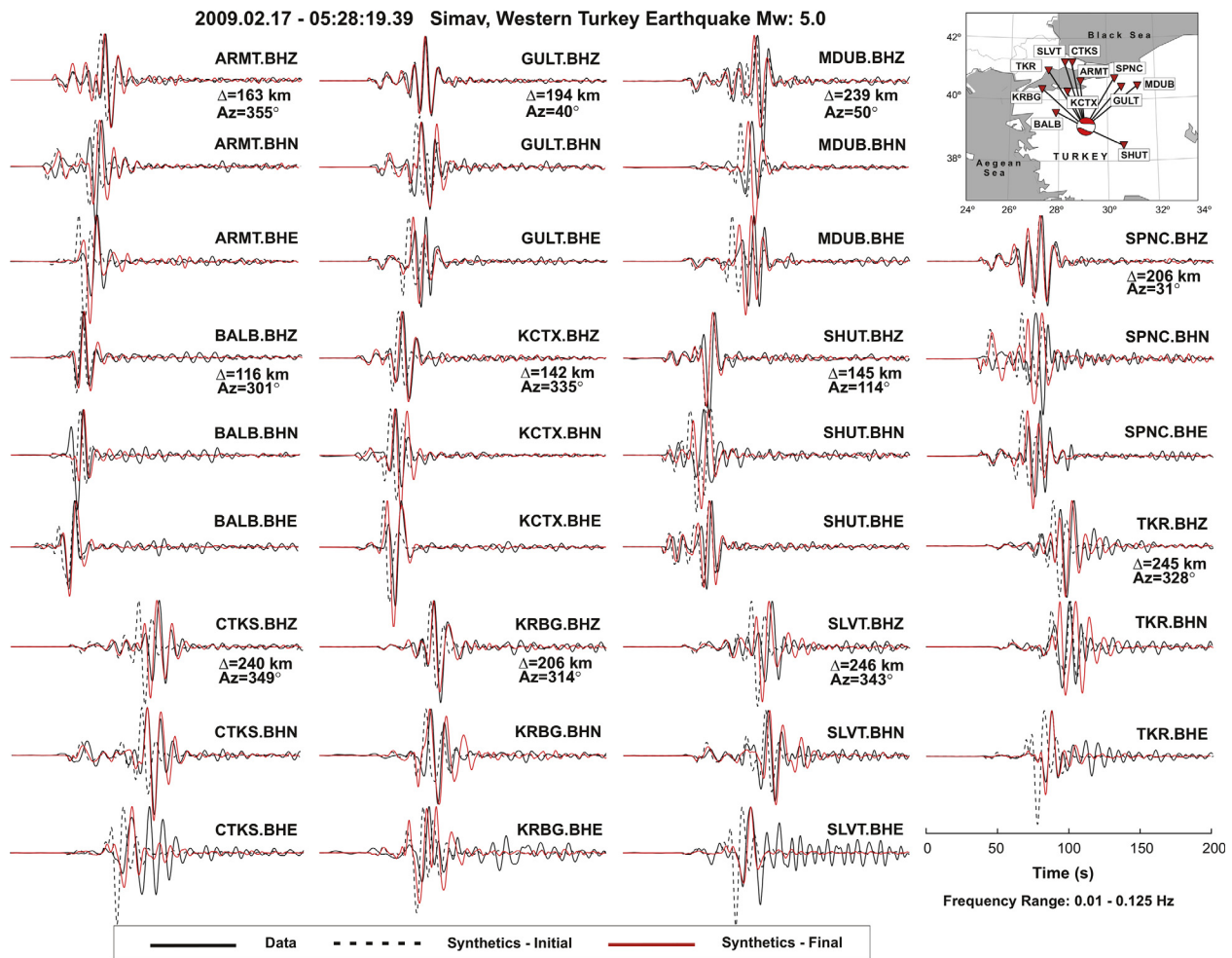


**Fig. 8.** Waveform comparison of the February 17, 2009–05:28 ( $M_w$ : 5.0) Simav (western Turkey) earthquake. Three-component velocity seismograms of each station are displayed for the BHZ, BHN and BHE channels, respectively. Observed data are plotted with solid black lines. Synthetic waveforms are represented with dashed black and solid red lines for the initial and final 3-D Earth models, respectively. Epicenter distance and azimuth information are indicated below each vertical component seismogram. Amplitudes are normalized and all waveforms are filtered between 8 and 100 s. (For interpretation of the references to colour in this figure legend, the reader is referred to the web version of this article.)

resolution in the vertical direction can unfortunately not be computed with the random probing technique (Fichtner and van Leeuwen, 2015). However, the comparison of crustal thickness in our model, with crustal thicknesses reported by previous receiver function studies, indicate that the vertical resolution of both methods is similar, i.e. around few kilometers (see Section 6.2).

#### 4.2. Waveform fits

In this section, waveform comparisons between initial and final 3-D Earth models, as well as synthetic tests for model validation and data predictability are presented. An additional set of waveform comparisons is displayed in the [Supplementary Online Material](#).

Waveform comparisons were performed for selected earthquake-station pairs that sample the study area along differently oriented ray paths. The final model is able to explain body and surface waveforms from 8 to 100 s period significantly better than the initial model. For most events, traveltimes are matched to within 1 s or less, and amplitudes to within 10% of their maximum. We observe the least significant improvements for events located close to the boundaries of the modelling domain, where Earth structure is less resolved. An exemplary waveform compar-

ison for the initial and the final models for the February 17, 2009 Simav earthquake ( $M_w$  5.0) is presented in Fig. 8.

To further assess the quality of the model, we compare observed and synthetic waveforms for six regional earthquakes that were not used in the inversion. Also for these additional events, the misfit for the final model ( $\chi_{19} = 1.14$ ) is significantly smaller than for the initial model ( $\chi_0 = 1.39$ ). These misfit values are similar to those obtained in the actual inversion, thus indicating that the data have not been overfit significantly. An example waveform comparison for the November 18, 2015 Çal-Denizli earthquake ( $M_w$  4.1) is presented in Fig. 9. Additional comparisons are shown in [Appendix A](#).

#### 5. Crustal and uppermost mantle structure

Our tomographic model provides new insight into 3-D variations of shear wave velocity and radial anisotropy to depths of  $\sim 30$ – $35$  km. Figs. 10 and 11 present the SH and SV velocity models, respectively. At upper-crustal depths, we infer the lowest SH velocities (2.3–3.2 km/s) beneath major fault zones, e.g., the NAFZ and its branches. SH velocities are low,  $\approx 2.6$ – $3.3$  km/s, in the Sea of Marmara, as well. In the upper crust, we constrain shear wave velocities of 2.9–3.3 km/s, and 3.1–3.4 km/s underneath the

20151118\_145540.08 Karapınar-Çal Denizli Earthquake Mw: 4.1

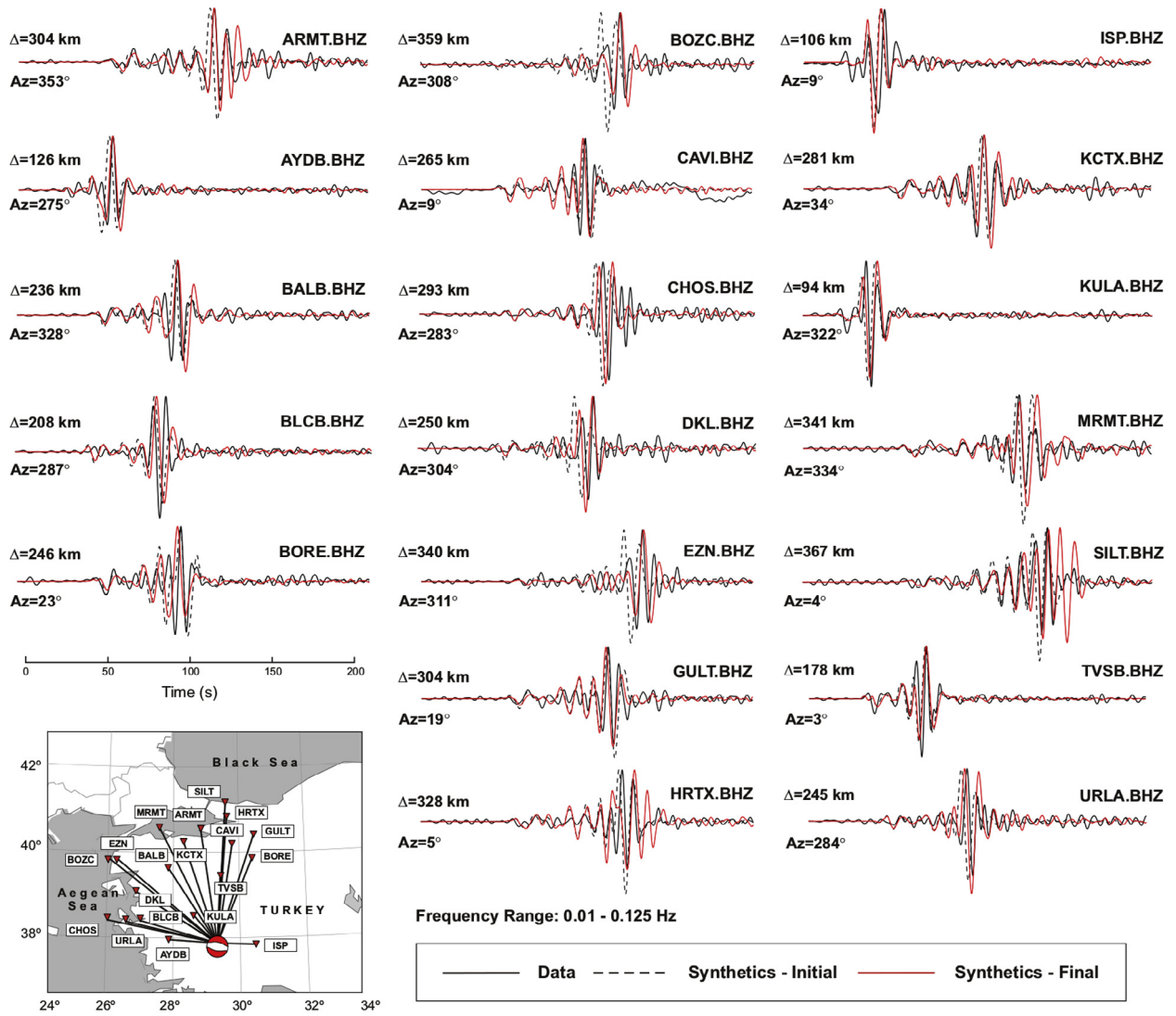


**Fig. 9.** Waveform comparison of the November 18, 2015–14:55 ( $M_w$ : 4.1) Çal-Denizli (southwest Turkey) earthquake. The velocity seismograms of each station are displayed for the BHZ channel. Observed data are plotted with solid black lines. Synthetic waveforms are represented with dashed black and solid red lines for the initial and final 3-D Earth models, respectively. Epicenter distance and azimuth information are indicated above and below each vertical component seismogram, respectively. Amplitudes are normalized and all waveforms are filtered between 8 and 100 s. (For interpretation of the references to colour in this figure legend, the reader is referred to the web version of this article.)

Kazdağ massif. At mid- to lower-crustal depth ranges, high SV velocity is found beneath the Kazdağ massif and surroundings (3.5–4.0 km/s). Further south, around the Menderes massif, we observe the highest SH wave velocities in the upper crust ( $\geq 3.3$  km/s), and corresponding SV wave velocities vary between 2.8 and 3.2 km/s. At mid- to lower crustal depth ranges, SH and SV wave velocities increase to  $\sim 4.0$  km/s beneath the Menderes massif.

To facilitate the geologic interpretation of our results in Section 6, the following paragraphs provide a more detailed analysis of the isotropic shear velocity and shear anisotropy.

5.1. Absolute isotropic S velocity

Fig. 12 displays a horizontal slice obtained from the 3-D isotropic shear velocity ( $V_s$ ) model at 5 km depth. In Appendix B, we additionally present horizontal depth slices throughout the

W-NW Turkey crust. The interpreted tectonic features and major city locations are indicated on the horizontal depth sections (Figs. 12 and 13). The color scale represents low to high absolute isotropic seismic velocities from dark red over white to dark blue (2.55–4.0 km/s), while black shades represent the upper mantle velocities from 4.0 to 5.0 km/s. We calculate the absolute isotropic S wave velocity from the SV and SH velocities as  $V_s^2 = \frac{2}{3}V_{SV}^2 + \frac{1}{3}V_{SH}^2$ .

In the upper part of the crust, we observe prominent low-velocity anomalies (2.55–3.2 km/s) beneath the NAFZ and the Sea of Marmara. Magnitudes of these low-velocity zones (LVZs) vary laterally along the NAFZ. For example, the strongest low-velocity anomaly of 2.55–2.8 km/s occurs above 10 km depth in the southwestern part of the Armutlu Peninsula where the southern branch of the NAFZ reaches into the sea through the Gulf of Gemlik. In the Gulf of Saros, low velocities of 2.7–3.2 km/s are recognized down to 15–20 km depth, which clearly marks the western continuation of the NAFZ.

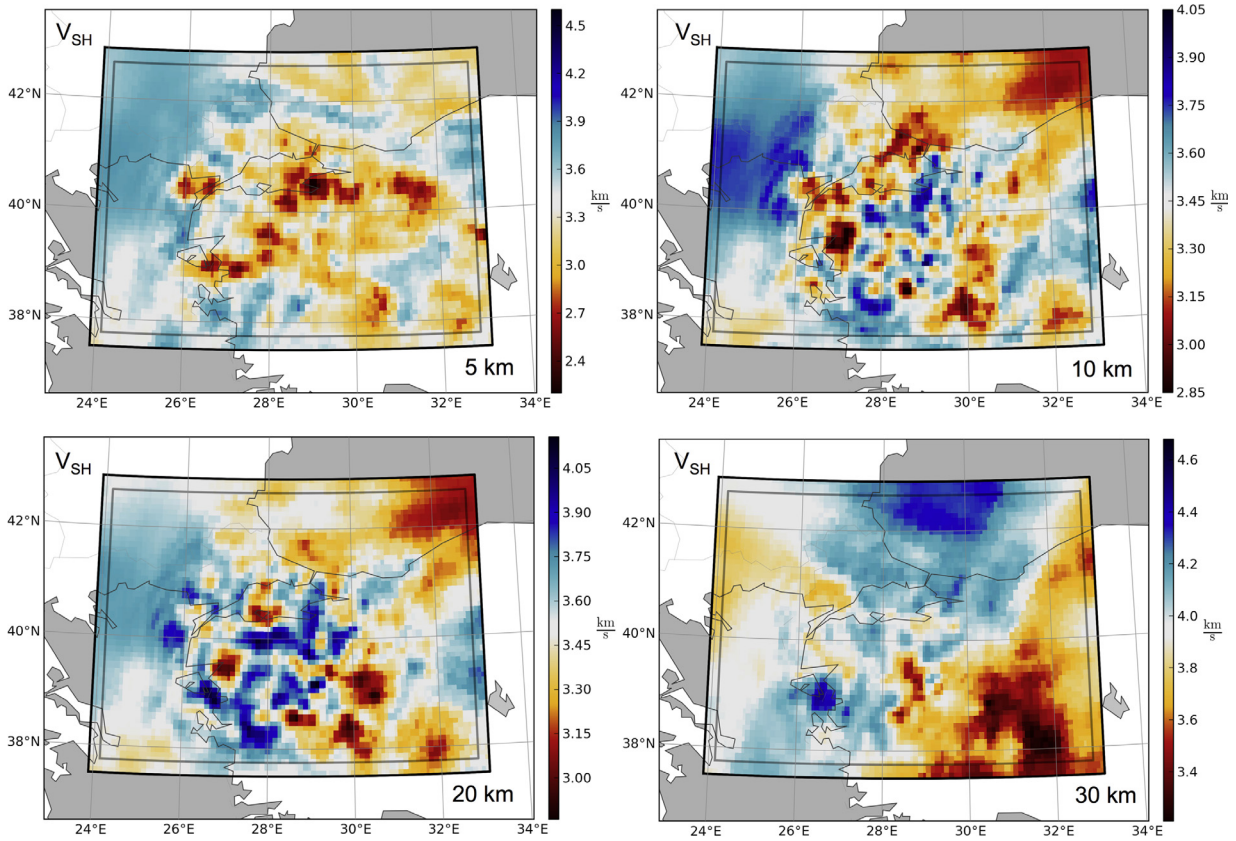


**Fig. 10.** Horizontal slices through the 3-D radially anisotropic Earth model of W-NW Turkey. SH wave velocity variations are shown for depths of 5–30 km. In each figure, depth labels are indicated in the lower right corners.

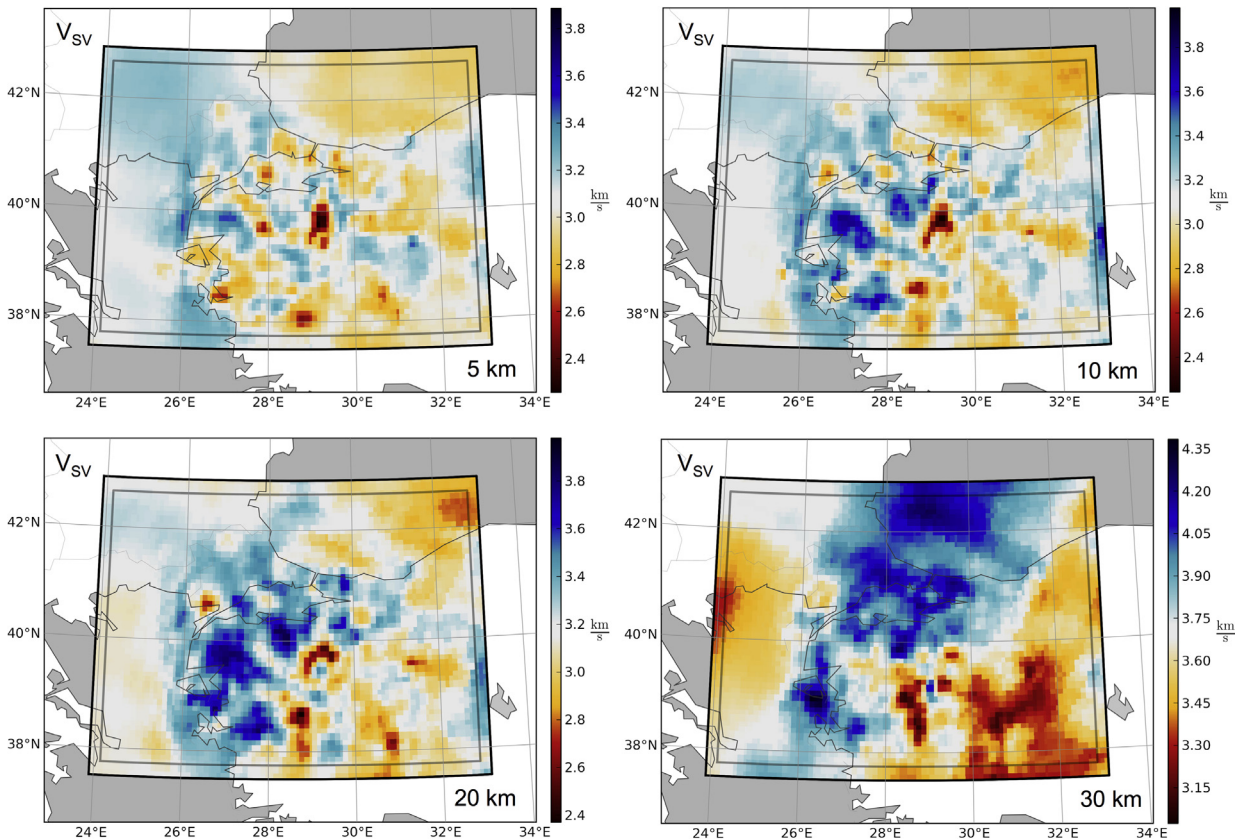


**Fig. 11.** Horizontal slices through the 3-D radially anisotropic Earth model of W-NW Turkey. SV wave velocity variations are shown for depths of 5–30 km. In each figure, depth labels are indicated in the lower right corners.

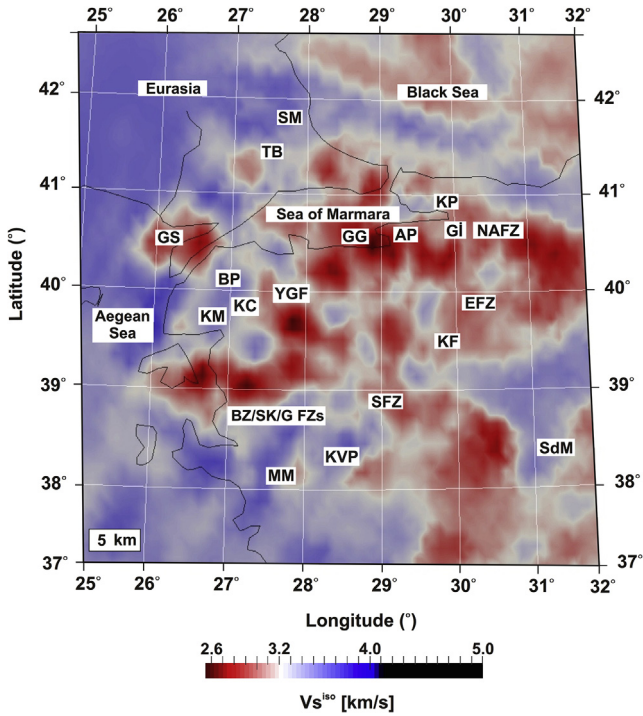


**Fig. 12.** Horizontal slice obtained from the absolute isotropic S wave velocity model ( $V_s$ ) of W-NW Turkey at 5 km depth. The color scale represents low to high isotropic S-wave velocities between dark red and white to dark blue shades ( $2.55 \leq V_s \leq 4.0$  km/s), while the upper mantle velocities are represented with black color between the  $4.0 < V_s \leq 5.0$  km/s range. Depth label is indicated in the lower left corner. Main tectonic features are labeled on top of the horizontal section. Abbreviations: AP: Armutlu Peninsula, BP: Biga Peninsula, BZ: Bergama-Zeytinadağ Fault Zone, EFZ: Eskişehir Fault Zone, GG: Gemenli Fault Zone, GI: Gulf of İzmit, GS: Gulf of Saros, KC: Karakaya Complex, KF: Kütahya Fault, KM: Kazdağ Massif, KP: Kocaeli Peninsula, KVP: Kula Volcanic Province, MM: Menderes Massif, NAFZ: North Anatolian Fault Zone, SdM: Sultandağ Mountain, SFZ: Simav Fault Zone, SM: Strandja Massif, SK: Soma-Kırkağaç Fault Zone, TB: Thrace Basin, YGF: Yenice-Gönen Fault Zone.

Below  $40^\circ\text{N}$ , low-velocity variations ( $2.55\text{--}2.9$  km/s) appear down to 14 km depth beneath the Bergama-Zeytinadağ FZ, the Soma-Kırkağaç FZ and the Gemenli FZ (W Turkey). We observe clear low-velocity signatures ( $2.7\text{--}3.2$  km/s) down to  $\sim 14$  km depth beneath the Simav region. Another distinct low-velocity zone ( $2.9\text{--}3.2$  km/s) is confined between 10 and 28 km depth beneath the Kula Volcanic Province ( $28.5^\circ\text{E}\text{--}38.6^\circ\text{N}$ ).

Striking high-velocity signatures ( $\geq 3.3$  km/s) are found beneath the Menderes and the Kazdağ massifs. We also infer prominent high velocities in the Armutlu Peninsula below 10 km depth. Shear wave velocities increase progressively, and the highest isotropic S wave velocities are found within the lower crust throughout the region ( $3.7\text{--}4.0$  km/s).

We further present vertical depth sections extracted from the 3-D absolute isotropic S-wave velocity model. The profile locations and the vertical cross-sections are shown in Figs. 13 and 14, respectively. Most vertical profiles display striking Moho undulations beneath W-NW Turkey.

5.2. Radial anisotropy

Fig. 15 displays the 3-D distribution of radial anisotropy from 5 to 30 km depth beneath W-NW Turkey. The radial anisotropy parameter  $\zeta$  is calculated as the difference between horizontally (SH) and vertically polarized (SV) shear wave velocities, normal-

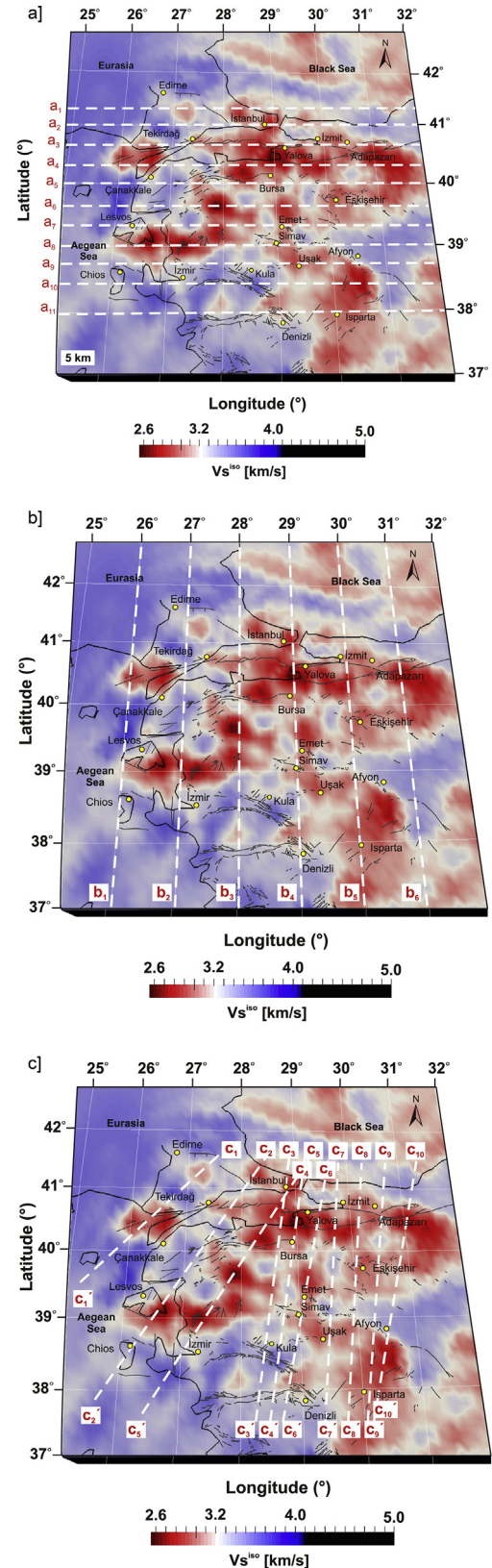


**Fig. 13.** The profile locations for vertical cross-sections are shown with thick white lines on the shallowest (5 km) absolute isotropic S wave velocity model a) for the E-W direction, b) for the N-S direction, and c) for the NE-SW direction. Thin black lines represent regional faults reported by Şaroğlu et al. (1992), and the yellow circles denote major city locations.

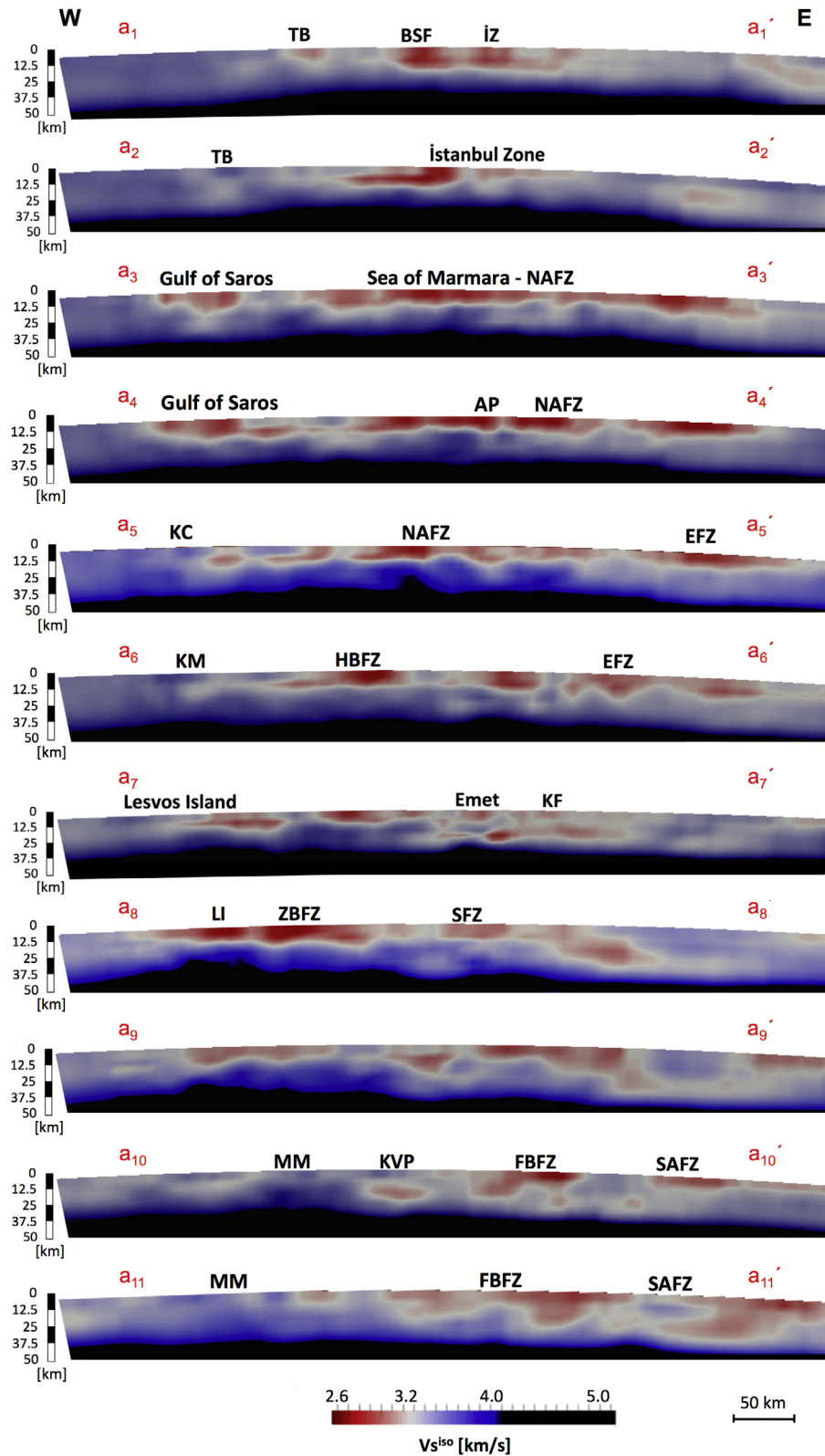


**Fig. 14.** Vertical depth profiles through the 3-D absolute isotropic S wave velocity model. a) E-W cross-sections, b) N-S cross-sections, c) NE-SW cross-sections. Profiles are extracted for depths down to 50 km. The color scale represents low to high isotropic S-wave velocities between dark red and white to dark blue shades ( $2.55 \leq V_s \leq 4.0$  km/s), while the upper mantle velocities are represented with black color between the  $4.0 < V_s \leq 5.0$  km/s range. Profile labels and main tectonic features are indicated on top of each cross-section. Abbreviations: AP: Armutlu Peninsula, BSF: Black Sea Fault, BP: Biga Peninsula, EFZ: Eskişehir Fault Zone, FBFZ: Fethiye-Burdur Fault Zone, GI: Gulf of İzmit, HBFZ: Havran-Balya-Balıkesir Fault Zone, İZ: İstanbul Zone, KC: Karakaya Complex, KF: Kütahya Fault, KM: Kazdağ Massif, KP: Kocaeli Peninsula, KVP: Kula Volcanic Province, LI: Lesvos Island, MM: Menderes Massif, NAFZ: North Anatolian Fault Zone, SAFZ: Sultandağ-Akşehir Fault Zone, SFZ: Simav Fault Zone, SM: Sea of Marmara, SZ: Sakarya Zone, TB: Thrace Basin, ZBFZ: Zeytinadağ-Bergama Fault Zone. (For interpretation of the references to colour in this figure legend, the reader is referred to the web version of this article.)

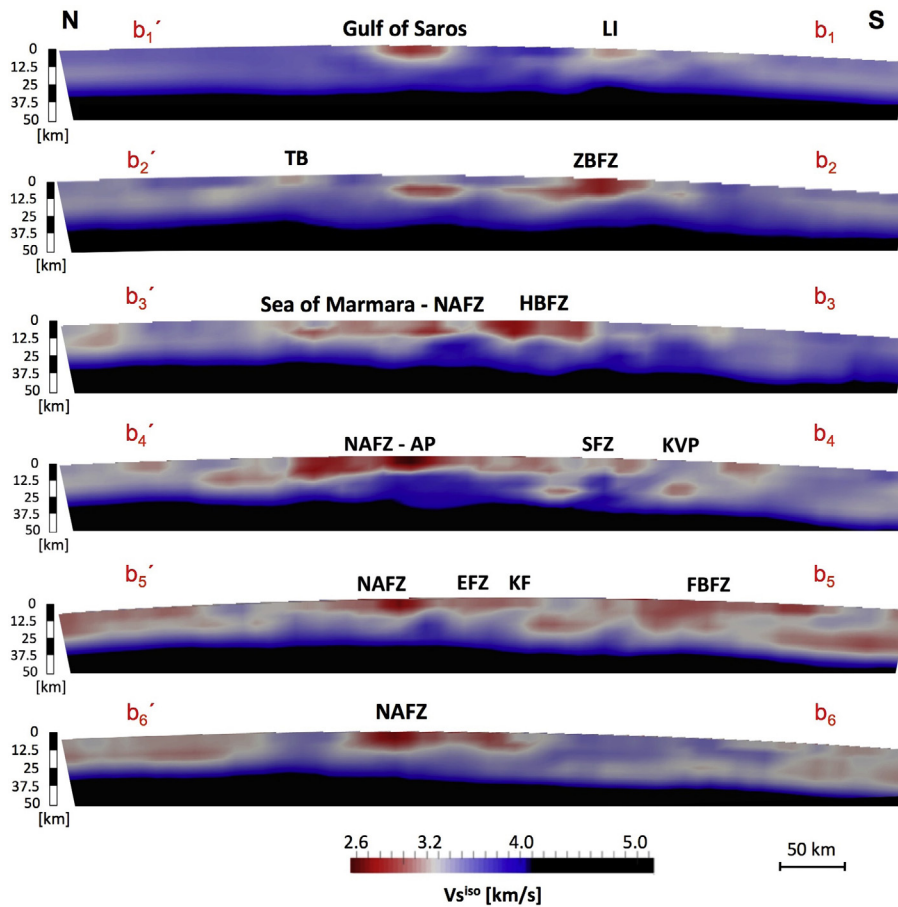


Fig. 14 (continued)

ized with the isotropic shear wave velocity, i.e.  $\zeta = (V_{SH} - V_{SV})/V_S$ . In each figure, the color scale ranges between  $-0.2 \leq \zeta \leq +0.2$ , indicating negative ( $V_{SV} > V_{SH}$ ) and positive ( $V_{SH} > V_{SV}$ ) radial anisotropy. The 3-D full-waveform tomography reveals a strong radial anisotropy in the W-NW Turkey crust of up to 20%. The strongest negative radial anisotropy is found in the upper crust, and it mostly emerges in the close vicinity of known weakness zones, e.g. the NAFZ and its segments around the Sea of Marmara and the Gulf of Saros. Another significant negative radial anisotropy patch (15–20%) is centered near  $27.25^\circ\text{E}$ – $39.7^\circ\text{N}$  around the Biga Peninsula between 15 and 25 km depth. We infer strong positive radial anisotropy (15–20%) beneath the Mendere Massif at upper crustal depth ranges. We also notice that radial anisotropy is mostly positive for greater depths (>20 km), and magnitude of the observed radial anisotropy drops below 10% in the mid to lower crust.

The strong radial anisotropy may indicate a high rate of deformation and heterogeneity in W-NW Turkey. The heavily fractured and fluid-saturated rocks, alignments of anisotropic minerals, heterogeneous isotropic layers, and crustal flow can generate the observed anisotropy patterns at different crustal depths (Babuska and Cara, 1990; Vergne et al., 2003; Sherrington et al., 2004; Mainprice, 2007). Since a quantitative distinction between the various factors that contribute to observed anisotropy is hardly possible (Wang et al., 2013; Fichtner et al., 2013c), its interpretation requires caution and additional inversions of combined geophysical, geological and petrological data.

## 6. Discussion

We discuss principal characteristics our 3-D radially anisotropic Earth model and its isotropic component in terms of the regional

geology, seismicity and other published geophysical studies for regions with sufficiently high resolution. The overall tectonic history of western Turkey has resulted in the formation of very complex crustal structure. The closure of the Neo-Tethyan oceanic basin was followed by post-orogenic extension and widespread magmatism in the region (Şengör and Yılmaz, 1981). On-going subduction of the African plate is also causing high-rate of crustal deformation and extension (20–30 mm/yr; Reilinger et al., 2006; McClusky et al., 2003).

The resolved features of our 3-D Earth model provide insight into diverse geological contrasts that evolved due to complex interactions of subduction roll-back, continental collision, extensional and strike-slip tectonics, block rotations, young and former magmatism (Oligocene-Neogene), high rate of fracturing and large-scale metamorphism.

### 6.1. Connection to surface-geological features

#### 6.1.1. Marmara Sea region

Several tectonic belts, active faulting, as well as geothermal areas encompass the Sea of Marmara and are expressed as heterogeneous subsurface structures. The transition between the E-W strike-slip character of the NAFZ and the N-S extensional regime of the Aegean further causes complex geometry and rotational movements in the region with a broad zone (~120 km; Şengör et al., 1985) of distributed deformation. Striking low-velocity signatures (2.6–3.2 km/s,  $V_{SH, SV}$ ) clearly mark these weakness zones along the NAFZ (Figs. 12, 13, and Appendix B). We mainly observe the low-velocity pattern within the tectonically active deep sedimentary basins (~5 km, Laigle et al., 2008) of the Sea of Marmara, in the Gulf of Saros (<15 km), and in the Armutlu Peninsula

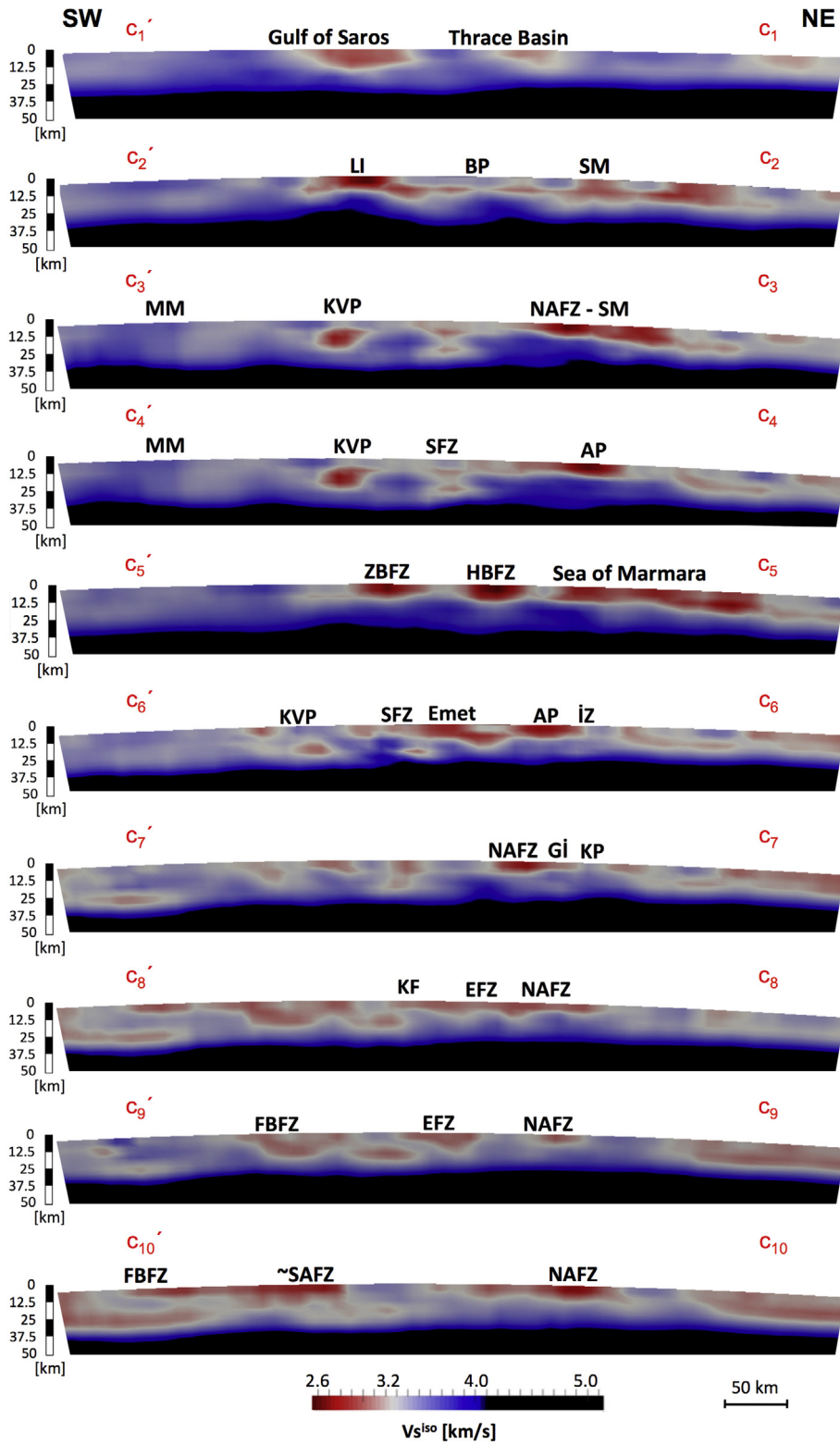
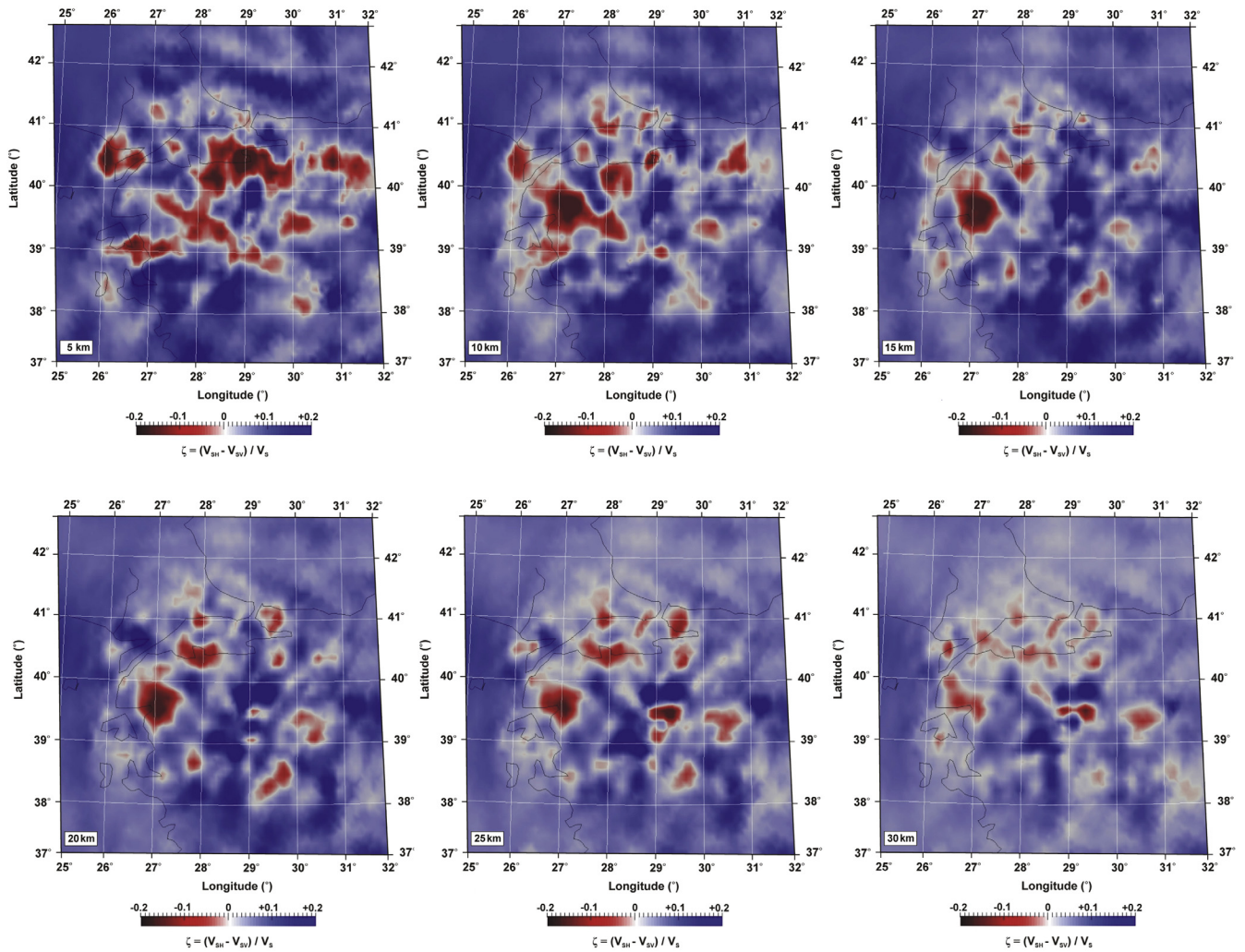


Fig. 14 (continued)

(<10–12 km). These results indicate that the upper crust is highly deformed and heavily fractured due to westward extrusion of the Anatolian Plate along the North Anatolian transform fault. Shear wave velocities are higher at mid-to-lower crust and resolved LVZs are within the reported seismogenic depths (~15 km;

Altuncu-Poyraz et al., 2015; Yolsal-Çevikbilen et al., 2012), which suggest a ductile behavior below the brittle upper crust.

The strong negative radial anisotropy (10–20%) in the S-SE Marmara (e.g. around the Armutlu Peninsula) and the Gulf of Saros extends down to 10–14 km depths. Based on shear wave splitting



**Fig. 15.** Horizontal slices showing the lateral variations of radial anisotropy in W-NW Turkey between 5 and 30 km depth. In each figure, the color scale ranges between the negative to positive radial anisotropy values between dark red and white to dark blue ( $-0.2 \leq \zeta \leq +0.2$ ) indicating the regions with high SV and SH wave speeds, respectively.

analysis, Eken et al. (2013) also pointed out the presence of anisotropy within the upper 10 km of the crust in the eastern Sea of Marmara region. This underlines that anisotropy tends to occur mostly within the upper crust, even though uniquely addressing its origins is hardly possible. Besides its strong anisotropic properties, the crust beneath the eastern Sea of Marmara significantly undulates with respect to its surroundings (Fig. 14 profiles  $a_{3,4}$ ,  $b_4$ ,  $c_{3,4}$ ). This undulating character of the Moho might be attributed to complex block rotations (e.g. Hergert et al., 2011) observed between two branches of the NAFZ and adjacent Armutlu Peninsula.

### 6.1.2. Kütahya-Simav Graben

Recent analysis of intensive seismicity (focal depths of ~9–15 km) revealed that the N-S extensional deformation is still prevailing in the Kütahya-Simav region (Taymaz et al., 2004; Yolsal-Çevikbilen et al., 2014). Active faulting (e.g. Simav detachment fault), granitic intrusions, magmatism, and also geothermal activity mainly characterize the Simav and surroundings. Reported heat flow values ( $110 \text{ mWm}^{-2}$ , İlkışık, 1995;  $220 \text{ mWm}^{-2}$ , compilation of Kılınç, 2004) are also remarkably higher than the world average ( $65 \text{ mWm}^{-2}$ , Pollack et al., 1993) due to the presence of a thin continental crust. Such high-temperature conditions can play a significant role to decrease seismic velocities and cause partial melting. We observe mid-to-lower crustal (20–29 km) relatively weak LVZs (2.9–3.2 km/s) between N-NW Simav, Emet and

Kütahya (e.g. Fig. 14,  $a_7$ ,  $b_{4,5}$ ,  $c_6$ ). The presence of partial melts might have a significant effect to decrease seismic velocities at greater depths in the region. The  $V_p/V_s$  ratio ( $>1.85$ ) analysis of Vanacore et al. (2013) also supports the idea of possible partial melting in the lower crust associated with the regional extension in western Turkey. Thus, the Kütahya-Simav and surroundings is a good example of weak nature of highly fractured, high temperature crust resulting in lowered seismic velocities.

### 6.1.3. Kazdağ (Biga peninsula), Menderes Massif

The Kazdağ and the Menderes massifs are metamorphic core complex features developed during the tectonic evolution of the W-NW Turkey crust. The resolved shear wave velocities ( $V_s > 3.3 \text{ km/s}$ ) of our model reflect metamorphic composition beneath those regions (Figs. 3, 12, and Appendix B). In the Menderes massif, the radial anisotropy is positive throughout the crust at all resolved depths mostly implying the horizontal alignment of anisotropic minerals under the extensional tectonics. In the Biga Peninsula, the strong negative patterns (10–20%) tend to occur below ~10 km depth down to the base of the crust. The Biga Peninsula comprises various tectonic units with different origins (e.g. oceanic assemblages, granitoid emplacements). The Late Oligocene metamorphic units of the Kazdağ Massif and strongly deformed metamorphic rocks of the Karakaya Complex dominate among these units (Pickett and Robertson, 1996; Okay and Satir, 2000; Okay

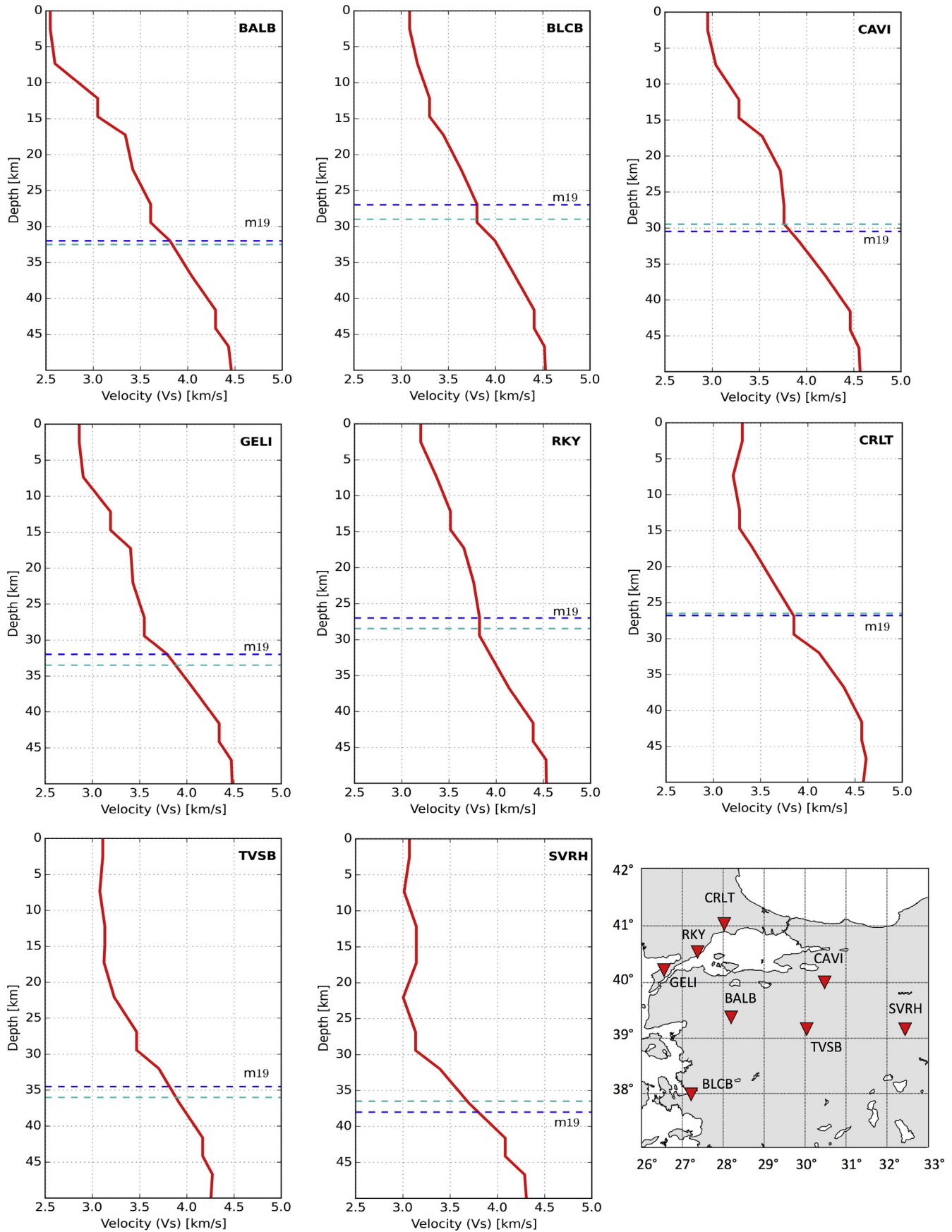


**Fig. 16.** 1-D isotropic S wave velocity–depth profiles extracted from the 3-D radially anisotropic Earth model. Blue and green dashed lines mark depths corresponding to  $V_s = 3.8$  km/s (final model,  $m_{19}$ ) and the Moho depth estimates of Vanacore et al. (2013), respectively. Station locations are displayed in the lower right corner. (For interpretation of the references to colour in this figure legend, the reader is referred to the web version of this article.)

and Göncüoğlu, 2004; Duru et al., 2004). The mid crustal negative radial anisotropy pattern in the Kazdağ massif and surroundings may have emerged from the deeper expression of pronounced strong lithological variations.

#### 6.1.4. Kula Volcanic Province (Uşak)

A prominent low-velocity anomaly and a positive radial anisotropy pattern (10–20%) exist between 10 and 28 km depth below the Kula volcanics (e.g. Figs. 12, 14, 15, profiles  $a_9$ ,  $a_{10}$ ,  $c_3$ ,  $c_4$ ,  $c_6$ ). There is a strong relation between the resolved deep LVZ and possible emplacement of a magmatic body beneath the Kula Volcanic Province (KVP). The KVP represents the youngest volcanism (Plio-Quaternary) in western Turkey (Richardson-Bunbury, 1996; Westaway et al., 2004) and different origins (e.g. upwelling of asthenospheric material, decompression melting) have been suggested by various studies (Richardson-Bunbury, 1996; Saunders et al., 1998; Alici et al., 2002; Tokçer et al., 2005; Grützner et al., 2013). Recently, tomographic models of Biryol et al. (2011) and Fichtner et al. (2013a) imaged low seismic velocities between ~75 and 300 km depths corresponding to the KVP. Biryol et al. (2011) interpreted this anomaly as a rapid upwelling of the asthenospheric material (Tokçer et al., 2005), which originates from the tear between the Cyprus and the Aegean slabs. Based on the previous implications, the resolved low-velocity anomaly is important to support the possible deployment of this hot material into the mid-to-lower crust as a result of slab tearing beneath the western Turkey. However, SH velocities faster than SV suggest a non-vertical flow beneath the crust underlying KVP. This LVZ might have resulted from horizontally aligned minerals in previously deployed magmatic material or melting rather than indicating ongoing vertical intrusion of deep magma (Figs. 14 and 15).

#### 6.2. Comparison with other tomography and receiver function studies

Seismic velocity properties of western Turkey have long been investigated using different data and methods (e.g. Barış et al., 2005; Akyol et al., 2006; Salah et al., 2007; Cambaz and Karabulut, 2010; Biryol et al., 2011; Mutlu and Karabulut, 2011; Salaün et al., 2012; Bakırcı et al., 2012; Yolsal-Çevikbilen et al., 2012; Delph et al., 2015). Here, we first provide a comparison to the initial model, presented and discussed in Fichtner et al. (2013b) and Govers and Fichtner (2016). This will be followed by a comparison to receiver function studies.

Our 3-D Earth model improves the shallow to deep crustal velocity structure of the initial model in W-NW Turkey thanks to the large quantity of newly added local earthquake data. Thus, three-component complete waveforms are explained significantly better with a total misfit reduction of 24% percent with respect to Fichtner et al. (2013b). The small-scale features, and the presence of deep and shallow LVZs (e.g. the Sea of Marmara, the Gulf of Saros, and the Kula Volcanic Province) became more distinctive throughout the iterations. Despite these refinements, our results are still in good agreement with the interpretation of the initial model by Govers and Fichtner (2016). They indicated low isotropic S wave anomalies beneath western Turkey and Aegean crust with respect to the global continental average ( $V_S \approx 3.75\text{--}3.90$  km/s). They defined average S wave velocities to be  $V_S \approx 3.6\text{--}3.7$  km/s for the middle crust, and  $V_S \approx 3.8\text{--}4.0$  km/s for the lower crust, which is compatible with our findings.

Further, we compare lower crustal average velocities ( $V_S > 3.8$  km/s, Christensen and Mooney, 1995) of our model with reported Moho depths. The crustal thickness of western Turkey has been investigated by a significant number of receiver function studies using different techniques and data (e.g. Vanacore et al., 2013; Karabulut et al., 2013; Kind et al., 2015). Vanacore et al. (2013) reported a thinned Moho with 30 km thickness beneath western

Turkey. Karabulut et al. (2013) implied 25–27 km Moho depth for the Sea of Marmara and the Menderes Massif, while Zor et al. (2006) indicated average Moho depths of 29–32 km for the Marmara region. Zhu et al. (2006) also estimated a crustal thickness around 28–30 km beneath the Menderes Massif. In Fig. 16, we present comparison of the 1-D velocity-depth profiles extracted from our 3-D Earth model beneath the arbitrarily selected receivers with the Moho depth estimates of Vanacore et al. (2013). For example, these comparisons yield 0.3 km difference for stations BALB and CRLT, 1.5 km for SVRH, and 2 km for BLCB station. These small differences indicate that our 3-D Earth model has comparable vertical resolution to receiver functions, and that it is largely consistent with previously reported Moho thicknesses in the region. The striking Moho undulations throughout western Turkey are also well resolved (Fig. 14) and consistent with recent observations of Karabulut et al. (2013).

## 7. Conclusions

In this paper, we present a 3-D radially anisotropic shear wave velocity model of the W-NW Turkey crust and uppermost mantle based on full-waveform tomography. Our model provides new insight into the three-dimensional crustal S, SH and SV wave velocity variations and radial anisotropy patterns. Results indicate the complex tectonic evolution of the region, and are generally in good agreement with other reported geological and geophysical studies (e.g. heat flow, tomography, receiver function, seismicity). The principle findings of this study are summarized as follows: [1] In the upper crust, the isotropic shear wave velocities are strikingly low (2.55–3.2 km/s) and likely to be associated with active faulting, young volcanism and elevated crustal temperatures due to extensional and strike slip tectonics. High-velocity characteristics are also very prominent in relation with the metamorphic massifs (e.g. Strandja, Kazdağ, and Menderes massifs). [2] In the mid-to-lower crust, velocities increase progressively with depth (3.4–4.0 km/s) except within several LVZs (e.g. Kula Volcanic Province, Simav-Emet region) indicating magmatism, high temperatures and partial melting in the deep crust. [3] Radial anisotropy is found to be very strong (~20%) throughout the upper crust, while its strength reduces with depth. [4] The undulating nature of the Moho discontinuity in almost all vertical sections reveals a complex subcrustal deformation beneath W-NW Turkey.

Our findings suggest that the 3-D radially anisotropic velocity model successfully marks zones that evolved as a result of active tectonics in the region. With our model, we anticipate to contribute to earthquake source mechanism inversion and localization efforts of small to moderate earthquakes in which proper 3-D variation of seismic velocity distributions are required (e.g. Hejrani et al., 2017). Future work may include refining regional complexities with adding more high-quality three-component data recorded in the Aegean Sea and central Anatolia. We expect to obtain moment tensor inversions of future regional earthquakes using three-component complete waveforms produced by our 3-D Earth model. We also would like to emphasize the importance of developing combined inversions of different observations (e.g. seismic velocity, density, temperature, petrological data, etc.) to better qualify the observed anisotropy in the future.

## Acknowledgements

This study is part of Ph.D. thesis by Yeşim Çubuk-Sabuncu (2016), which is supported by Istanbul Technical University Research Fund (İTÜ-FBE-BAP-Project No: 36969). It is further partly supported by International Graduate Fellowship program of TÜBİTAK (visiting scholarship during April–October 2013, ETH

Zurich, Switzerland) and EU-HORIZON-2020: COST Actions: Earth System Science and Environmental Management, ES1401-Time Dependent Seismology (TIDES): STSMs (Short Term Scientific Missions visiting scholarship, October 2015, ETH Zurich, Switzerland). We gratefully acknowledge support by the Swiss National Supercomputing Centre (CSCS) for allowing us to use the Piz Daint cluster. Furthermore, we thank Lion Krischer for the development of LASIF. Tuncay Taymaz acknowledges support from Turkish Academy of Sciences (TÜBA) in the framework for Young Scientist Award Program (TÜBA-GEBİP), Turkish National Scientific and Technological Research Council (TÜBİTAK) and Alexander von Humboldt Foundation (AvH). We would like to thank Tuna Eken, Erdinc Saygin, and Seda Yolsal-Çevikbilen for discussions and comments that helped us to improve the manuscript. The authors used

the SAC2000 package to process earthquake data, Generic Mapping Tools (GMT; [Wessel and Smith, 1998](#)), Paraview software ([Ahrens et al., 2005](#)), and ObsPy – a python toolbox for seismology ([Beyreuther et al., 2010](#)) to prepare some of the figures.

### Appendix A

In appendix A, we present waveform comparisons between observations, initial and final synthetics of example regional earthquakes, which are not used in the inversion process in order to validate accuracy of the final 3-D Earth model. Synthetic waveforms are calculated using both the initial and final 3-D Earth models. Results of waveform comparisons are displayed in appendix [Figs. A1–A5](#).

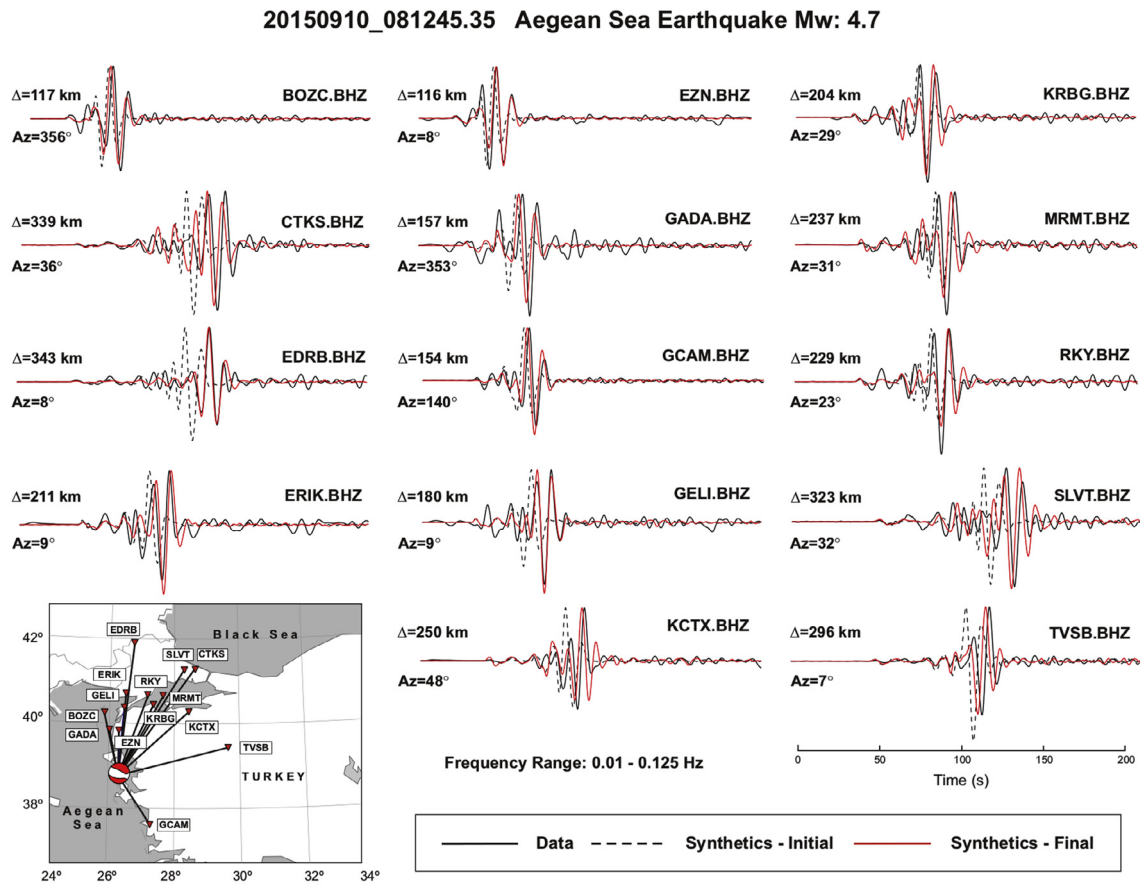


**Fig. A1.** Waveform comparison of the September 10, 2015 – 08:12 ( $M_w$ : 4.7) earthquake occurred in the Aegean Sea region at 15 km depth. The velocity seismograms of each station are displayed for the BHZ channel. Header information is as in [Fig. 9](#).

20150918\_223028.0 TEPEBAŞI-ESKİŞEHİR Earthquake Mw: 3.7

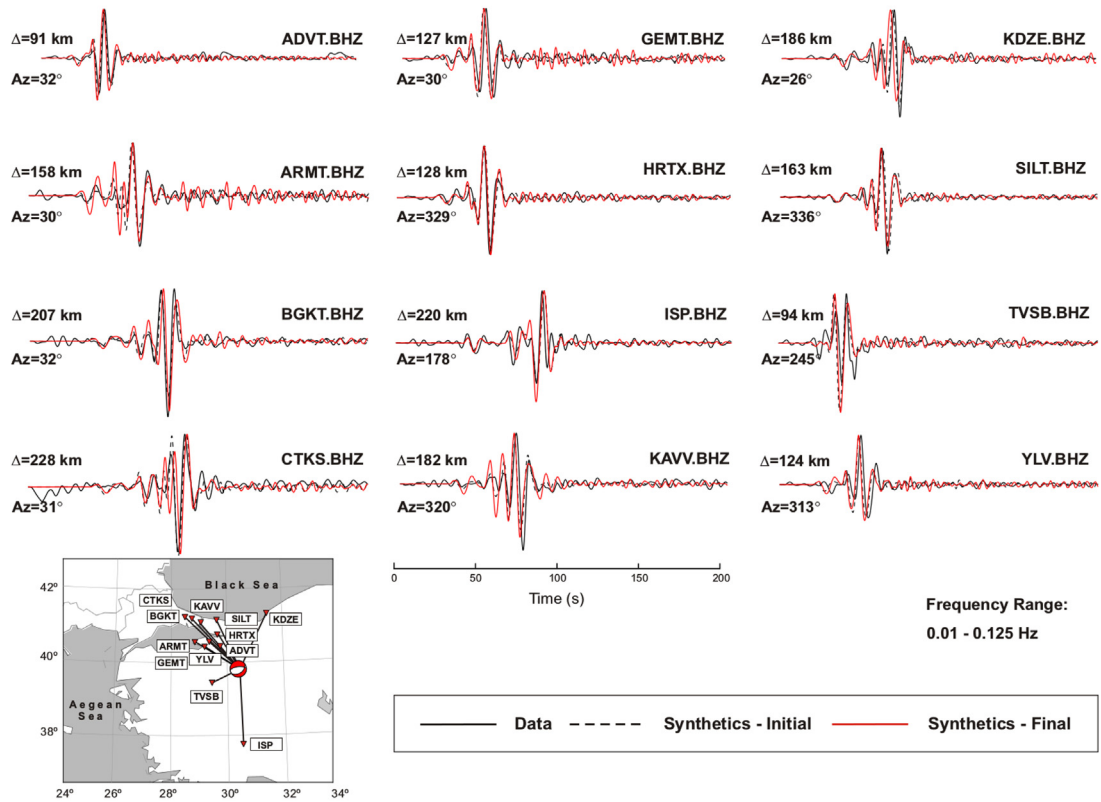


Fig. A2. Waveform comparison of the September 18, 2015 – 22:30 ( $M_w$ : 3.7) earthquake occurred in the Tepebaşı-Eskişehir region at 7 km depth. The velocity seismograms of each station are displayed for the BHZ channel. Header information is as in Fig. 9.

20150922\_071110.0 Inlice-Simav Earthquake Mw: 4.1

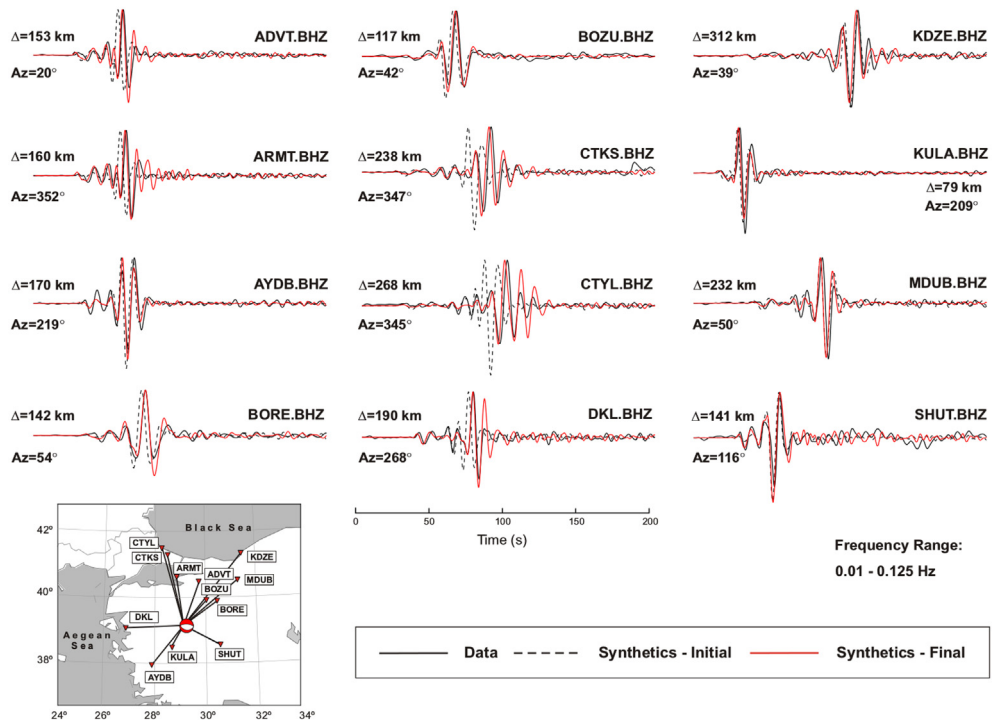


Fig. A3. Waveform comparison of the September 22, 2015 – 07:11:10.0 ( $M_w$ : 4.1) earthquake occurred in the İnce-Simav region at 9 km depth. The velocity seismograms of each station are displayed for the BHZ channel. Header information is as in Fig. 9.

20151013\_231810.0 Ahlatlıçesme - Kütahya Earthquake Mw: 4.0

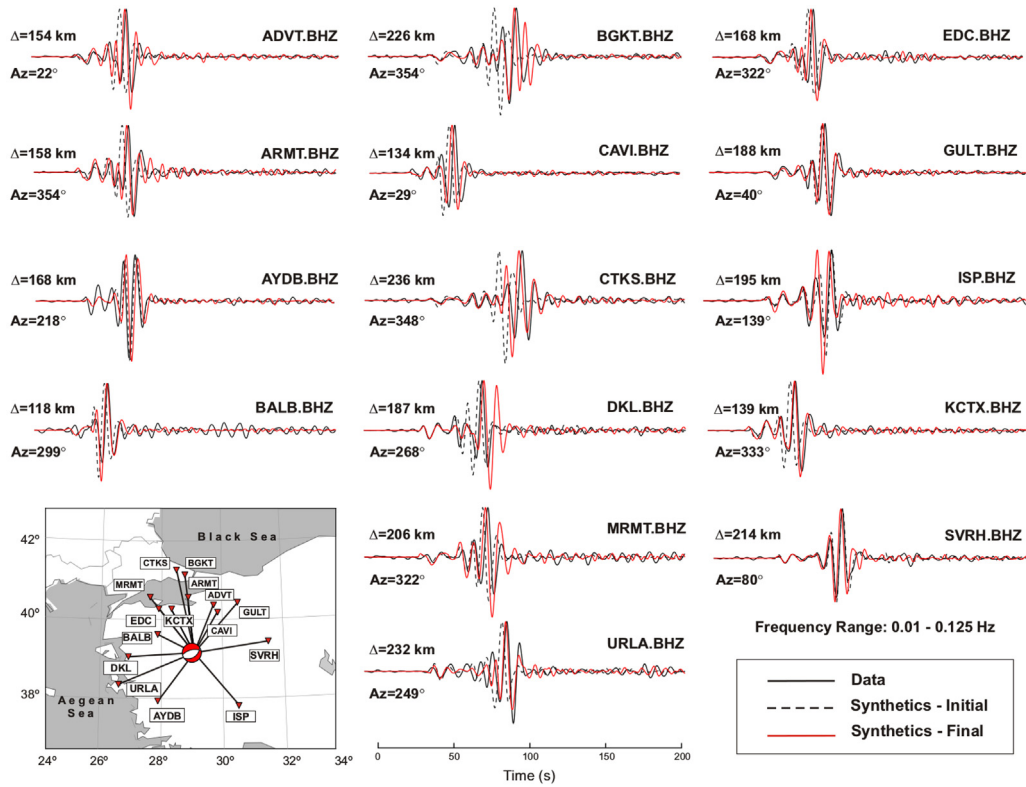


Fig. A4. Waveform comparison of the October 13, 2015 – 23:18 ( $M_w$ : 4.0) earthquake occurred in the Ahlatlıçesme region at 9 km depth. The velocity seismograms of each station are displayed for the BHZ channel. Header information is as in Fig. 9.

20151116\_154543.48 Sea of Marmara Earthquake Mw: 3.9

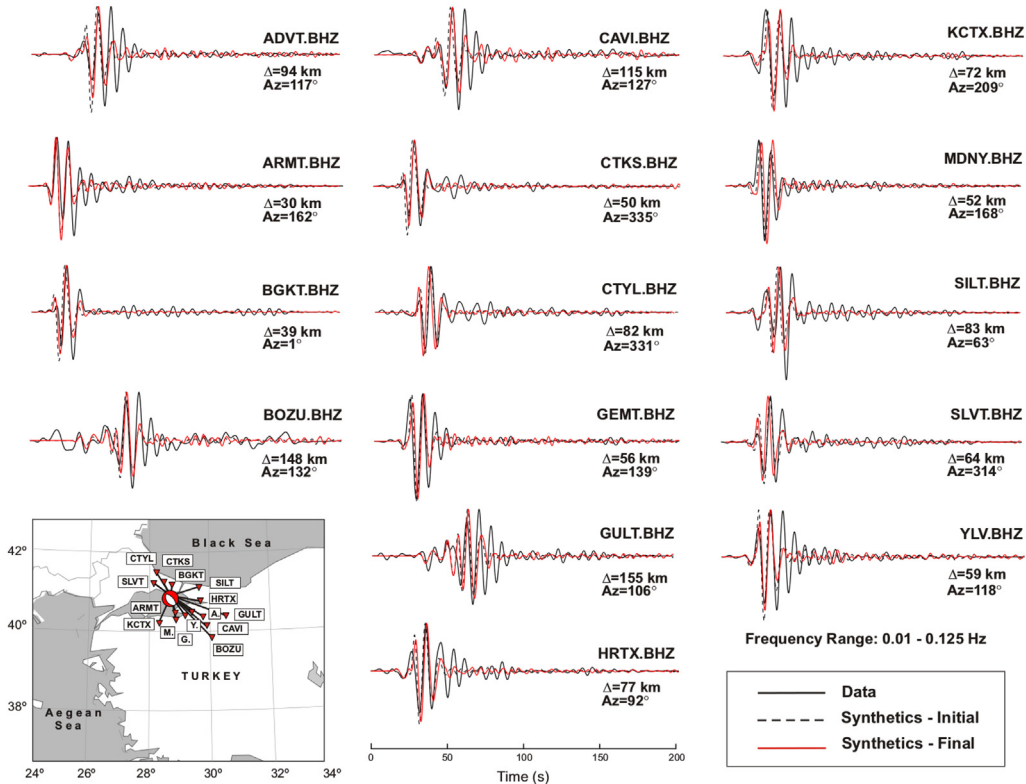
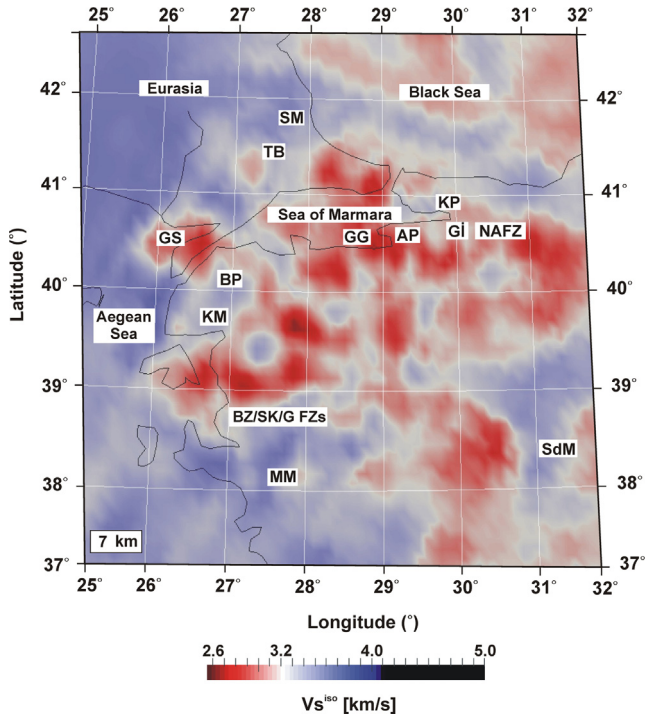


Fig. A5. Waveform comparison of the November 16, 2015 – 15:45 ( $M_w$ : 3.9) earthquake occurred in the Sea of Marmara region at 7.7 km depth. The velocity seismograms of each station are displayed for the BHZ channel. Header information is as in Fig. 9.

**Appendix B**

In appendix B, we present horizontal depth slices through the absolute isotropic S wave velocity model ( $V_s$ ) of W-NW Turkey crust and upper-most mantle between 7 and 35 km depth. In each horizontal depth section (Figs. B1–B7), the color scale represents

low to high isotropic S wave velocities between dark red and white to dark blue shades ( $2.55 \leq V_s \leq 4.0$  km/s), while the upper mantle velocities are represented with black color between the  $4.0 < V_s \leq 5.0$  km/s range. Depth labels are indicated in the lower left corner. Main tectonic features are labeled on top of the each horizontal section. Abbreviations: AP: Armutlu Peninsula, BP: Biga



**Fig. B1.** Horizontal slice obtained at 7 km depth from the absolute isotropic S wave velocity model ( $V_s$ ) of W-NW Turkey crust and upper-most mantle.

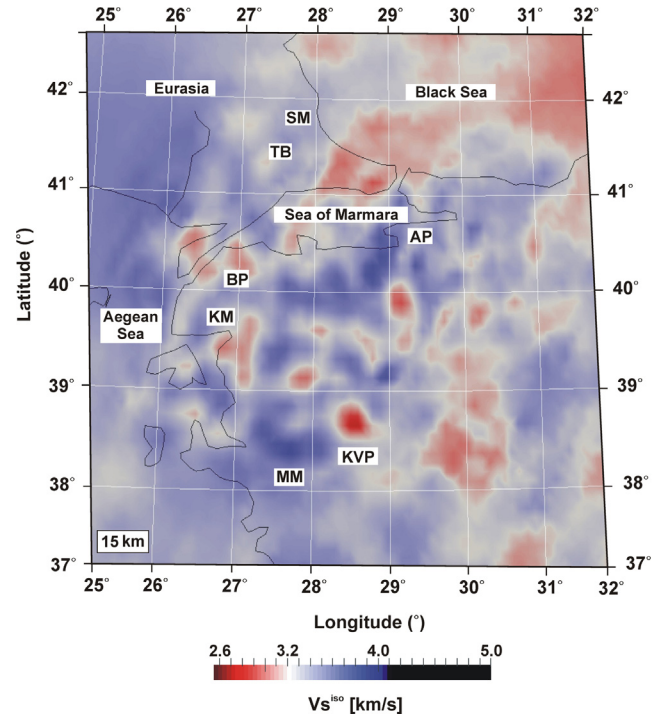


**Fig. B3.** Horizontal slice obtained at 15 km depth from the absolute isotropic S wave velocity model ( $V_s$ ) of W-NW Turkey crust and upper-most mantle.

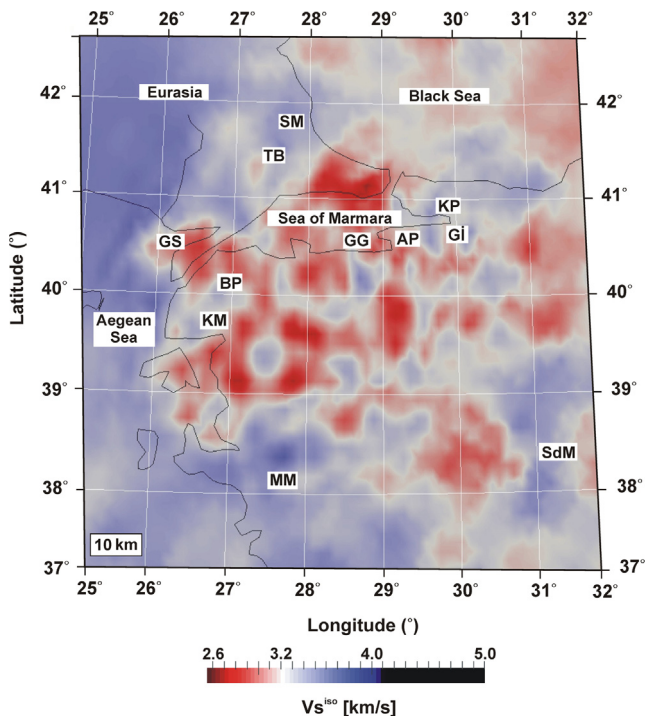


**Fig. B2.** Horizontal slice obtained at 10 km depth from the absolute isotropic S wave velocity model ( $V_s$ ) of W-NW Turkey crust and upper-most mantle.

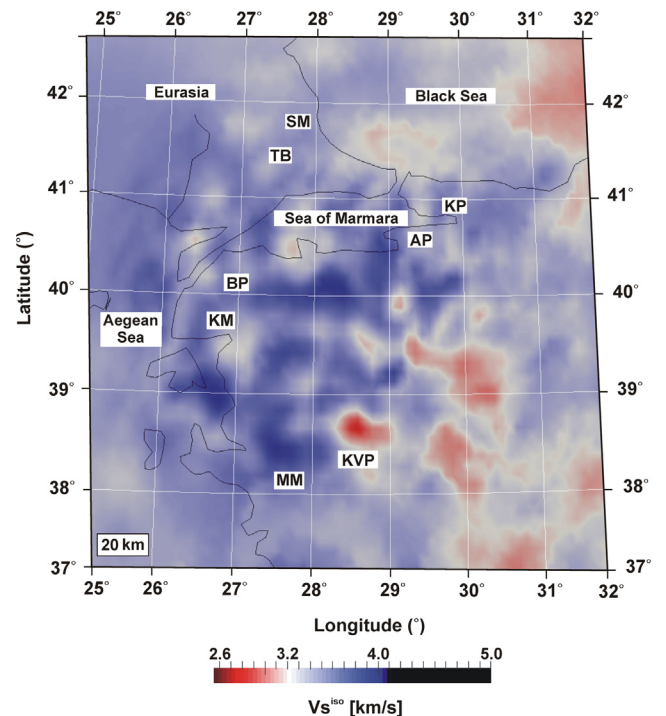


**Fig. B4.** Horizontal slice obtained at 20 km depth from the absolute isotropic S wave velocity model ( $V_s$ ) of W-NW Turkey crust and upper-most mantle.

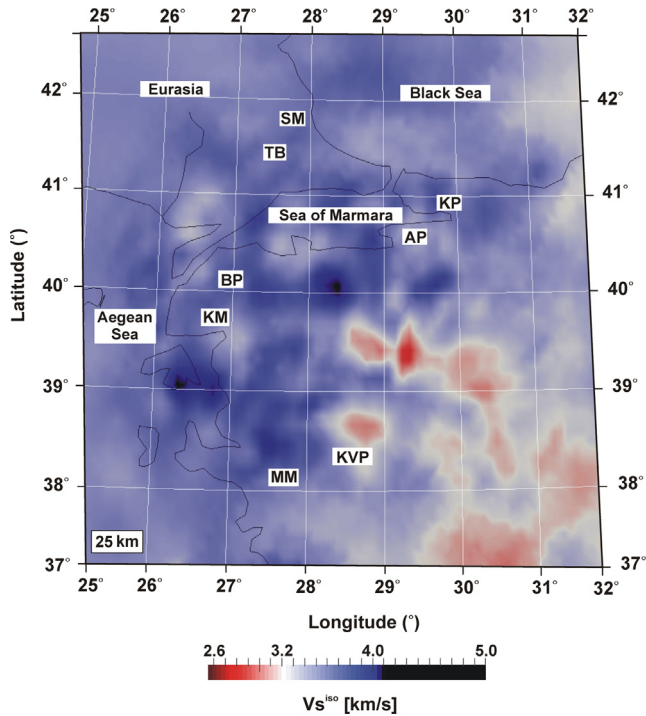


Fig. B5. Horizontal slice obtained at 25 km depth from the absolute isotropic S wave velocity model ( $V_s$ ) of W-NW Turkey crust and upper-most mantle.

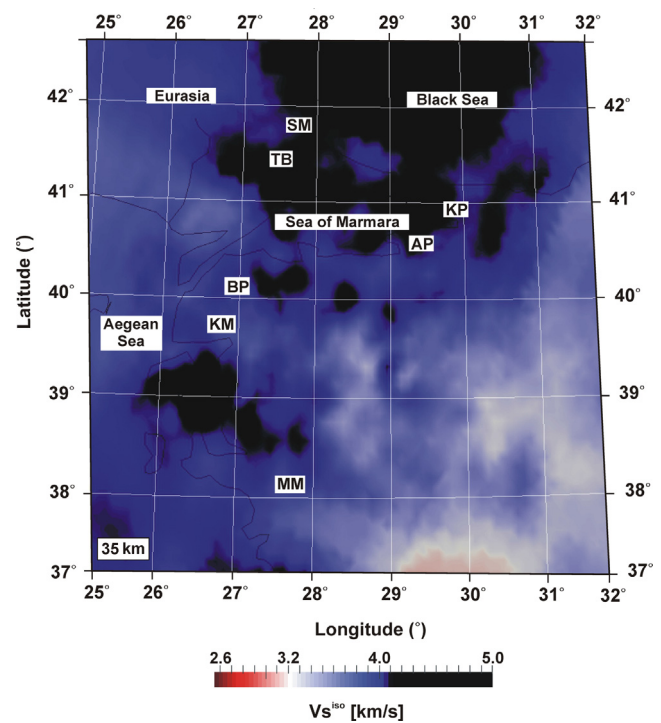


Fig. B7. Horizontal slice obtained at 35 km depth from the absolute isotropic S wave velocity model ( $V_s$ ) of W-NW Turkey crust and upper-most mantle.

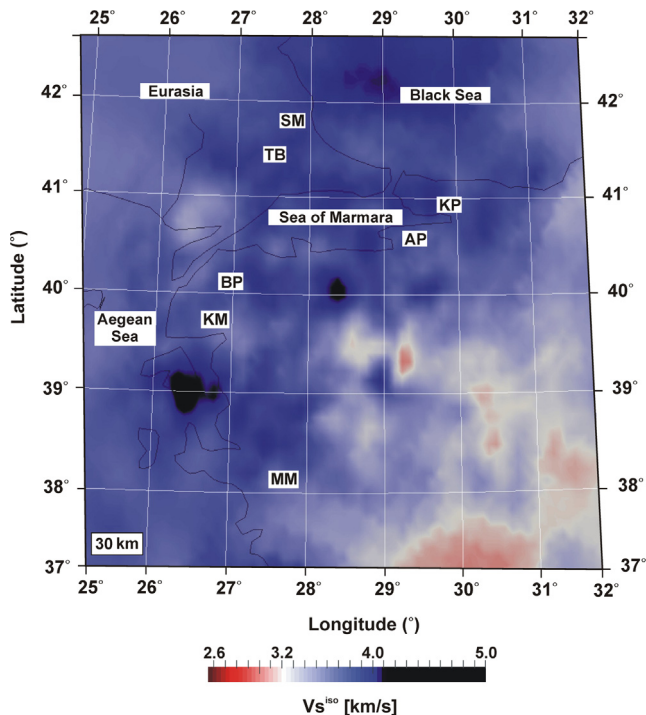


Fig. B6. Horizontal slice obtained at 30 km depth from the absolute isotropic S wave velocity model ( $V_s$ ) of W-NW Turkey crust and upper-most mantle.

Peninsula, BZ: Bergama-Zeytinadağ Fault Zone, G: Gelenbe Fault Zone, GG: Gulf of Gemlik, Gİ: Gulf of İzmit, GS: Gulf of Saros, KM: Kazdağ Massif, KP: Kocaali Peninsula, KVP: Kula Volcanic Province, MM: Mendere Massif, NAFZ: North Anatolian Fault Zone, SdM: Sultandağı Mountain, SM: Strandja Massif, SK: Soma-Kırkağaç Fault Zone, TB: Thrace Basin.

## Appendix C. Supplementary data

Supplementary data associated with this article can be found, in the online version, at <http://dx.doi.org/10.1016/j.pepi.2017.06.014>.

## References

- Ahrens, J., Geveci, B., Law, C., 2005. ParaView: An End-User Tool for Large Data Visualization, Visualization Handbook. Elsevier. ISBN-13: 978-0123875822.
- Aksu, A.E., Hall, J., Yalıtırak, C., 2008. Miocene-recent evolution of anaximander mountain and Finike Basin at the junction of Hellenic and Cyprus Arcs, Eastern Mediterranean. *Marine Geol.* <http://dx.doi.org/10.1016/j.margeo.2008.04.008>.
- Akyol, N., Zhu, L., Mitchell, B.J., Sözbilir, H., Kekovalı, K., 2006. Crustal structure and local seismicity in western Anatolia. *Geophys. J. Int.* 166, 1259–1269.
- Alıcı, P., Temel, A., Gourgaud, A., 2002. Pb–Nd–Sr isotope and trace element geochemistry of Quaternary extension-related alkaline volcanism: a case study of Kula region (western Anatolia, Turkey). *J. Volcanol. Geotherm. Res.* 243/7, 1–24.
- Altuncu-Poyraz, S., Teoman, M.U., Türkelli, N., Kahraman, M., Cambaz, D., Mutlu, A., Rost, S., Houseman, G.A., Thompson, D.A., Cornwell, D., Utku, M., Gülen, L., 2015. New constraints on micro-seismicity and stress state in the western part of the North Anatolian Fault Zone: Observations from a dense seismic array. *Tectonophysics* 656, 190–201.
- Altunkaynak, Ş., Yıldırım, D., Genç, C.Ş., Sunal, G., Gertisser, R., Furnes, H., Foland, K. A., Yang, J., 2012. Spatial, temporal and geochemical evolution of Oligo–Miocene granitoid magmatism in western Anatolia, Turkey. *Gondwana Res.* 21, 961–986.
- Babuska, V., Cara, M., 1990. Seismic Anisotropy in the Earth. *Modern Approaches in Geophysics*, vol. 10. Springer, ISBN 978-94-010-5596-3.
- Bakırcı, T., Yoshizawa, K., Özer, M.F., 2012. Three dimensional S wave structure of the upper mantle beneath Turkey from surface wave tomography. *Geophys. J. Int.* 190, 1058–1076. <http://dx.doi.org/10.1111/j.1365-246X.2012.05526.x>.
- Barış, S., Nakajima, J., Hasegawa, A., Honkura, Y., Ito, A., Uçer, B., 2005. The three-dimensional structure of  $V_p$ ,  $V_s$  and  $V_p/V_s$  in the upper crust of the Marmara region, NW Turkey. *Earth Planets Space* 57 (11), 1019–1038.
- Beyreuther, M., Barsch, R., Krischer, L., Megies, T., Behr, Y., Wassermann, J., 2010. ObsPy: A python toolbox for seismology. *Seism. Res. Lett.* 81 (3), 530–533. <http://dx.doi.org/10.1785/gssrl.81.3.530>.
- Biryol, C.B., Beck, S.L., Zandt, G., Özacar, A.A., 2011. Segmented African lithosphere beneath the Anatolian region inferred from teleseismic P-wave tomography. *Geophys. J. Int.* 184, 1037–1057.
- Cambaz, D.M., Karabulut, H., 2010. Love-wave group velocity maps of Turkey and surrounding regions. *Geophys. J. Int.* 181, 502–520. <http://dx.doi.org/10.1111/j.1365-256X.2010.04516.x>.
- Chen, P., Zhao, L., Jordan, T.H., 2007. Full 3D tomography for the crustal structure of the Los Angeles region. *Bull. Seis. Soc. Am.* 97, 1094–1120.

- Christensen, N.J., Mooney, W.D., 1995. Seismic velocity structure and composition of the continental crust: a global view. *J. Geophys. Res.* 100 (B6), 9761–9788.
- Colli, L., Fichtner, A., Bunge, H.-P., 2013. Full waveform tomography of the upper mantle in the South Atlantic region: Imaging westward fluxing shallow asthenosphere? *Tectonophysics* 604, 26–40.
- Confal, J., Eken, T., Tilmann, F., Yolsal-Çevikbilen, S., Çubuk-Sabuncu, Y., Saygin, E., Taymaz, T., 2016. Investigation of Mantle Kinematics beneath the Hellenic-Subduction Zone with Teleseismic Direct Shear Waves. *Phys. Earth Planet. Inter.* 261, 141–151.
- Çubuk, Y., Yolsal-Çevikbilen, S., Taymaz, T., 2014. Source parameters of the 2005–2008 Bala-Sırapınar (central Turkey) earthquakes: Implications for the internal deformation of the Anatolian plate. *Tectonophysics* 635, 125–153.
- Delph, J., Biryol, B.C., Beck, S., Zandt, G., Ward, K.M., 2015. Shear wave velocity structure of the Anatolian Plate: anomalously slow crust in southwestern Turkey. *Geophys. J. Int.* 202, 261–276.
- Dewey, J.F., Hempton, M.R., Kidd, W.S.F., Şaroğlu, F., Şengör, A.M.C., 1986. Shortening of continental lithosphere: the neotectonics of Eastern Anatolia – a young collision zone. *Collision Tectonics. Spec. Publ. geol. SOC. London*, vol. 19. Blackwell Scientific Publications, Oxford, pp. 3–36.
- Durek, J.J., Ekström, G., 1996. A radial model of an elasticity consistent with long-period surface wave attenuation. *Bull. seism. Soc. Am.* 86, 144–158.
- Duru, M., Pehlivan, Ş., Şentürk, Y., Yavaş, F., Kar, H., 2004. New Results on the lithostratigraphy of the Kazdağ Massif in Northwest Turkey. *Turk. J Earth Sci.* 13, 177–186.
- Endrun, B., Lebedev, S., Meier, T., Tirel, C., Friederich, W., 2011. Complex layered deformation within the Aegean crust and mantle revealed by seismic anisotropy. *Nat. Geosci.* 4, 203–207.
- Fichtner, A., van Leeuwen, T., 2015. Resolution analysis by random probing. *Geophys. Res., Solid Earth* 120. <http://dx.doi.org/10.1002/2015JB012106>.
- Fichtner, A., Bunge, H.P., Igel, H., 2006a. The adjoint method in seismology – I. Theory. *Phys. Earth Planet. Int.* 157, 86–104.
- Fichtner, A., Bunge, H.P., Igel, H., 2006b. The adjoint method in seismology – II. Applications: traveltimes and sensitivity functionals. *Phys. Earth Planet. Int.* 157, 105–123.
- Fichtner, A., Kennett, B.L.N., Igel, H., Bunge, H.P., 2008. Theoretical background for continental- and global-scale full-waveform inversion in the time–frequency domain. *Geophys. J. Int.* 175, 665–685.
- Fichtner, A., Kennett, B.L.N., Igel, H., Bunge, H.P., 2009a. Full seismic waveform tomography for upper-mantle structure in the Australasian region using adjoint methods. *Geophys. J. Int.* 179, 1703–1725.
- Fichtner, A., Kennett, B.L.N., Igel, H., Bunge, H.P., 2009b. Spectral-element simulation and inversion of seismic waves in a spherical section of the Earth. *J. Numer. Anal. Ind. Appl. Math.* 4, 11–22.
- Fichtner, A., Kennett, B.L.N., Igel, H., Bunge, H.P., 2010. Full waveform tomography for radially anisotropic structure: new insight into present and past states of the Australasian upper mantle. *Earth Planet. Sci. Lett.* 290, 270–280.
- Fichtner, A., Trampert, J., Cupillard, P., Saygin, E., Taymaz, T., Capdeville, Y., Villaseñor, A., 2013a. Multiscale full waveform inversion. *Geophys. J. Int.* 194, 534–556. <http://dx.doi.org/10.1093/gji/ggt118>.
- Fichtner, A., Saygin, E., Taymaz, T., Cupillard, P., Capdeville, Y., Trampert, J., 2013b. The deep structure of the North Anatolian Fault Zone. *Earth Planet. Sci. Lett.* 373, 109–117. <http://dx.doi.org/10.1016/j.epsl.2013.04.027>.
- Fichtner, A., Kennett, B.L.N., Trampert, J., 2013c. Separating intrinsic and apparent anisotropy. *Phys. Earth and Planet. Int.* 219, 11–20.
- Fielding, E.J., Lundgren, P.R., Taymaz, T., Yolsal-Çevikbilen, S., Owen, S.E., 2013. Fault-slip source models for the 2011 M 7.1 Van Earthquake in Turkey from SAR Interferometry, Pixel Offset Tracking, GPS and seismic waveform analysis. *Seism. Res. Lett.* 84, 579–593.
- Fletcher, R., Reeves, C.M., 1964. Function minimization by conjugate gradients. *Comput. J.* 7, 149–154.
- Gao, F., 2004. Waveform Tomography and its Application at a Groundwater Contamination Site (PhD thesis). Rice University, Houston, Texas, USA, pp. 152.
- Gokhberg, A., Fichtner, A., 2016. Full-waveform inversion on heterogeneous HPC systems. *Comp. Geosci.* 89, 260–268.
- Govers, R., Fichtner, A., 2016. Signature of slab fragmentation beneath Anatolia from full-waveform tomography. *Earth Planet. Sci. Lett.* 450, 10–19. <http://dx.doi.org/10.1016/j.epsl.2016.06.014>.
- Grützner, T., Prelevic, D., Akal, C., 2013. Geochemistry and origin of ultramafic enclaves and their basanitic host rock from Kula Volcano, Turkey. *Lithos* 180–181, 58–73.
- Hall, J., Aksu, A.E., Yaltrak, C., Winsor, J.D., 2008. Structural architecture of Rhodes basin: A deep decoupled that evolved since the Pliocene at the junction of Hellenic and Cyprus Arcs, Eastern Mediterranean. *Marine Geolo.* <http://dx.doi.org/10.1016/j.margeo.2008.02.007>.
- Hejrani, B., Tkalcic, H., Fichtner, A., 2017. Centroid moment tensor catalogue using a 3D continental scale Earth model: Application to earthquakes in Papua New Guinea and the Solomon Islands. *J. Geophys. Res.*, under review.
- Hergert, T., Heidbach, O., Bécel, A., Laigle, M., 2011. Geomechanical model of the Marmara Sea region-I. 3-D contemporary kinematics. *Geophys. J. Int.* 185, 1073–1089.
- Hestenes, M.R., Stiefel, E.L., 1952. Methods of conjugate gradients for solving linear systems. *J. Res. Nat. Bur. Stand.* 49, 409–436.
- İlkişik, O.M., 1995. Regional heat flow in western Anatolia using silica temperature estimates from thermal springs. *Tectonophysics* 244, 175–184.
- Karabulut, H., Paul, A., Ergün, T.A., Hatzfeld, D., Childs, D.M., Aktar, M., 2013. Long-wavelength undulations of the seismic Moho beneath the strongly stretched Western Anatolia. *Geophys. J. Int.* 194 (1), 450–464.
- Kılınc, H., 2004. Heat flow study in the Western Anatolia. Graduate Thesis, Istanbul Technical University, the Faculty of Mines, Department of Geophysical Engineering, Istanbul.
- Kind, R., Eken, T., Tilmann, F., Sodoudi, F., Taymaz, T., Bulut, F., Yuan, X., Can, B., Schneider, F., 2015. Thickness of the lithosphere beneath Turkey and surroundings from S-receiver functions. *Solid Earth* 6, 971–984.
- Kissling, E., Ellsworth, W.L., Eberhart-Phillips, D., Kradolfer, U., 1994. Initial reference models in local earthquake tomography. *J. Geophys. Res.* 99, 19635–19646.
- Krischer, L., Fichtner, A., Zukauskaitė, S., Igel, H., 2015. Large Scale Seismic Inversion Framework. *Seismol. Res. Lett.* 86 (4), 1198–1207. <http://dx.doi.org/10.1785/0220140248>.
- Laigle, M., Becel, A., De Voogd, B., Hirn, A., Taymaz, T., Özalaybey, S., 2008. A first deep seismic survey in the Sea of Marmara: deep basins and whole crust architecture and evolution. *Earth planet. Sci. Lett.* 270 (3–4), 168–179.
- Liu, Q., Tromp, J., 2006. Finite-frequency kernels based on adjoint methods. *Bull. Seis. Soc. Am.* 96, 2383–2397.
- Mainprice, D., 2007. Seismic anisotropy of the deep Earth from a mineral and rock physics perspective. In: Schubert, G. (Ed.), *Treatise on Geophysics*, vol. 2, pp. 437–492.
- Masclé, J., Martin, L., 1990. Shallow structure and recent evolution of the Aegean Sea: a synthesis based on continuous reflection profiles. *Mar. Geol.* 94, 271–299.
- McClusky, S.C., Reilinger, R., Mahmoud, S., Ben Sari, D., Teable, A., 2003. GPS constrains on Africa (Nubia) and Arabia plate motions. *Geophys. J. Int.* 155, 126–138.
- McKenzie, D., 1972. Active tectonics of the Mediterranean Region. *Geophys. J. R. Astr. Soc.* 30, 109–185.
- Meulenkamp, J.E., Wortel, W.J.R., Van Wamel, W.A., Spakman, W., Hoogerduyn-Strating, E., 1988. On the Hellenic subduction zone and geodynamic evolution of Crete in the late middle Miocene. *Tectonophysics* 146, 203–215.
- Mutlu, A.K., Karabulut, H., 2011. Anisotropic Pn tomography of Turkey and adjacent regions. *Geophys. J. Int.* 187, 1743–1758.
- Okay, A.I., 2008. Geology of Turkey: a synopsis. *Anschnitt, Zeitschrift für Kunst und Kultur im Bergbau, Veröff entlichungen aus dem Deutschen Bergbau-Museum Bochum* 157, Beiheft 21, 19–42.
- Okay, A.I., Gönçüoğlu, M.C., 2004. The karakaya complex: a review of data and concepts. *Turk. J. Earth Sci.* 13, 77–95.
- Okay, A.I., Satır, M., 2000. Upper Cretaceous Eclogite-Facies Metamorphic Rocks from the Biga Peninsula. Northwest Turkey. *Turkish J. Earth Sci.* 9, 47–56.
- Okay, A.I., Satır, M., 2006. Geochronology of Eocene plutonism and metamorphism in northwest Turkey: evidence for a possible magmatic arc. *Geodin. Acta* 19, 251–266.
- Okay, A.I., Tüysüz, O., 1999. Tethyan sutures of northern Turkey. In: Durand, B., Jolivet, L., Horvath, F., Seranne, M. (Eds.), *The Mediterranean Basins: Tertiary Extension Within the Alpine Orogen*, vol. 156. Geological Society, Special Publications, London, pp. 475–515.
- Pickett, E.A., Robertson, A.H.F., 1996. Formation of the Late Palaeozoic-Early Mesozoic Karakaya Complex and related ophiolites in NW Turkey by Palaeotethyan subduction-accretion. *J. Geol. Soc. London* 153, 995–1009.
- Pollack, H., Hurter, S.J., Johnson, J.R., 1993. Heat flow from the Earth's interior: Analysis of the global data set. *Rev. Geophys.* 31 (3), 267–280.
- Reilinger, R., McClusky, S., Vernant, P., Lawrence, S., Ergintav, S., Çakmak, R., Ozener, H., Kadirov, F., Guliev, I., Stepanyan, R., Nadariya, M., Hahubia, G., Mahmoud, S., Sakr, K., ArRajehi, A., Paradissis, D., Al-Aydrus, A., Prilepin, M., Guseva, T., Evren, E., Dmitrova, A., Filikov, S.V., Gomez, F., Al-Ghazzi, R., Karam, G., 2006. GPS constraints on continental deformation in the Africa–Arabia, Eurasia continental collision zone and implications for the dynamics of plate interactions. *J. Geophys. Res. Solid Earth* 111, B05411.
- Richardson-Bunbury, J.M., 1996. The Kula volcanic field, western Turkey: the development of a Holocene alkali basalt province and the adjacent normal-faulting graben. *Geol. Mag.* 133, 275–283.
- Rickers, F., Fichtner, A., Trampert, J., 2013. The Iceland-Jan Mayen plume system and its impact on mantle dynamics in the North Atlantic region: Evidence from full-waveform inversion. *Earth Planet. Sci. Lett.* 367, 39–51.
- Salah, M.K., Şahin, S., Kaplan, M., 2007. Seismic Velocity Structure along the Western Segment of the North Anatolian Fault Zone Imaged by Seismic Tomography. *Bull. Earthq. Res. Inst. Univ. Tokyo* 82, 209–223.
- Salauin, G., Pedersen, H., Paul, A., Farra, V., Karabulut, H., Hatzfeld, D., Papazachos, C., Childs, D.M., Pequegnat, C., SIMBAAT Team, 2012. High-resolution surface wave tomography of the Aegean-Anatolia region: constraints on upper mantle structure. *Geophys. J. Int.* 190, 406–420.
- Saunders, P., Priestley, K., Taymaz, T., 1998. Variations in the crustal structure beneath western Turkey. *Geophys. J. Int.* 134 (2), 373–389.
- Şaroğlu, F., Emre, Ö., Kuşçu, İ., 1992. Active Fault Map of Turkey, 2 Sheets, General Directorate of Mineral Research and Exploration – GDMRAE, Ankara, Turkey.
- Şengör, A.M.C., 1979. The North Anatolian transform fault: its age, offset and tectonic significance. *J. Geol. Soc. London* 136, 269–282.
- Şengör, A.M.C., Yılmaz, Y., 1981. Tethyan evolution of Turkey: a plate tectonic approach. *Tectonophysics* 75, 181–241.
- Şengör, A.M.C., Görür, N., Şaroğlu, F., 1985. Strike-slip faulting and related basin formation in zones of tectonic escape: Turkey as a case study. In: Biddle, K.T.,

- Christie-Blick (Eds.), *Strike-slip Deformation, Basin Formations and Sedimentation*, vol. 37. Soc. Econ. Paleontol. Mineral. Spec. Publ., pp. 227–264.
- Sherrington, H.F., Zandt, G., Frederiksen, A., 2004. Crustal fabric in the Tibetan plateau based on waveform inversions for seismic anisotropy parameters. *J. Geophys. Res.* 109, B02312.
- Tape, C., Liu, Q., Maggi, A., Tromp, J., 2010. Seismic tomography of the southern California crust based upon spectral-element and adjoint methods. *Geophys. J. Int.* 180, 433–462.
- Tarantola, A., 1984. Inversion of seismic reflection data in the acoustic approximation. *Geophysics* 49, 1259–1266.
- Taymaz, T., 1996. S-P-wave travel-time residuals from earthquakes and lateral inhomogeneity in the upper mantle beneath the Aegean and the Aegean Trench near Crete. *Geophys. J. Int.* 127, 545–558.
- Taymaz, T., Price, S., 1992. The 1971 May 12 Burdur earthquake sequence, SW Turkey: a synthesis of seismological and geological observations. *Geophys. Journ. Int.* 108, 589–603.
- Taymaz, T., Jackson, J., McKenzie, D., 1991. Active tectonics of the north and central Aegean sea. *Geophys. J. Int.* 106, 433–490.
- Taymaz, T., Jackson, J.A., Westaway, R., 1990. Earthquake mechanisms in the Hellenic Trench near Crete. *Geophys. J. Int.* 102, 695–731.
- Taymaz, T., Westaway, R., Reilinger, R., 2004. Active faulting and crustal deformation in the Eastern Mediterranean region. *Tectonophysics* 391 (1–4), 375. <http://dx.doi.org/10.1016/j.tecto.2004.07.005>.
- Taymaz, T., Yilmaz, Y., Dilek, Y., 2007. The geodynamics of the Aegean and Anatolia: introduction. *Geol. Soc. Lond. Spec. Publ.* 291, 1–16. ISBN: 978-1-86239-239-7.
- Teixeira, F.L., Chew, W.C., 1997. Systematic derivation of anisotropic pml absorbing media in cylindrical and spherical coordinates. *IEEE Microw. Guided Wave Lett.* 7 (11), 371–373.
- Tokcaer, M., Agostini, S., Savaşçın, M.Y., 2005. Geotectonic Setting and Origin of the Youngest Kula Volcanics (Western Anatolia), with a New Emplacement Model. *Turkish J. Earth Sci.* 14, 145–166.
- Van Hinsbergen, D.J.J., Dekkers, M.J., Bozkurt, E., Koopman, M., 2010. Exhumation with A Twist: Paleomagnetic Constraints on the Evolution of the Mendere Metamorphic Core Complex (Western Turkey). *Tectonics* 29.
- Vanacore, E.A., Taymaz, T., Saygin, E., 2013. Moho structure of the Anatolian Plate from receiver function analysis. *Geophys. J. Int.* 193, 329–337. <http://dx.doi.org/10.1093/gji/ggs107>.
- Vergne, J., Wittlinger, G., Farra, V., Su, H., 2003. Evidence for upper crustal anisotropy in the SongpanGanze (northeastern Tibet) terrane. *Geophys. Res. Lett.* 30. <http://dx.doi.org/10.1029/2002GL016847>.
- Wang, N., Montagner, J.-P., Fichtner, A., Capdeville, Y., 2013. Intrinsic versus extrinsic anisotropy: The radial anisotropy in reference Earth models. *Geophys. Res. Lett.* 40, 4284–4288.
- Wessel, P., Smith, W.H.F., 1998. New, improved version of the Generic Mapping Tools released. *EOS Trans. AGU* 79, 579.
- Westaway, R., Pringle, M., Yurtmen, S., Demir, T., Bridgland, D., Rowbotham, G., Maddy, D., 2004. Pliocene and Quaternary regional uplift in western Turkey: the Gediz River terrace staircase and the volcanism at Kula. *Tectonophysics* 391, 121–169.
- Yılmaz, Y., Genç, S.C., Güler, Ö.F., Bozcu, M., Yılmaz, K., Karacık, Z., Altunkaynak, S., Elmas, A., 2000. When did the western Anatolian grabens begin to develop? *Geological Society London Special Publications* 173 (1), 353–384.
- Yolsal, S., 2008. Source Mechanism Parameters and Slip Distributions of Crete-Cyprus Arcs, Dead Sea Transform Fault Earthquakes and Historical Tsunami Simulations. PhD Thesis, 523 pages, Graduate School of Institute of Science and Technology, Istanbul Technical University, November 2008, Istanbul, Turkey.
- Yolsal-Çevikbilen, S., 2014. Seismic anisotropy along the Cyprian arc and northeast Mediterranean Sea inferred from shear wave splitting analysis. *Phys. of the Earth and Planet. Int.* 233, 112–134.
- Yolsal-Çevikbilen, S., Taymaz, T., 2012. Earthquake source parameters along the Hellenic subduction zone and numerical simulations of historical tsunamis in the Eastern Mediterranean. *Tectonophysics* 536–537, 61–100.
- Yolsal-Çevikbilen, S., Taymaz, T., Helvacı, C., 2014. Earthquake mechanisms in the Gulfs of Gökova, Sığacık, Kuşadası, and the Simav Region (western Turkey): Neotectonics, seismotectonics and geodynamic implications. *Tectonophysics* 635, 100–124. <http://dx.doi.org/10.1016/j.tecto.2014.05.001>.
- Yolsal-Çevikbilen, S., Biryol, B.C., Beck, S., Zandt, G., Taymaz, T., Adıyaman, H., Özacar, A., 2012. 3-D Crustal Structure along the North Anatolian Fault Zone in north-central Anatolia revealed by local earthquake tomography. *Geophys. J. Int.* 188, 819–849. <http://dx.doi.org/10.1111/j.1365-246X.2011.05313.x>.
- Zheng, Y., Huang, X., 1997. Anisotropic perfectly matched layers for elastic waves in cartesian and curvilinear coordinates. MIT Earth Resources Laboratory, Consortium Report 18.
- Zhu, L., Mitchell, B.J., Akyol, N., Çemen, I., Kekovalı, K., 2006. Crustal thickness variations in the aegean region and implications for the extension of continental crust. *J. Geophys. Res.* 111.
- Zhu, H., Bozdogan, E., Tromp, J., 2015. Seismic structure of the European upper mantle based on adjoint tomography. *Geophys. J. Int.* 201, 18–52.
- Zor, E., Özalaybey, S., Gürbüz, C., 2006. The crustal structure of the eastern Marmara region, Turkey by teleseismic receiver functions. *Geophys. J. Int.* 167, 213–222.